

AD-A133 331

Contract No. N00019-81-C-0179

ATC Report No. R-92000/3CR-9

①

**THE EFFECT OF ENVIRONMENT ON
THE MECHANICAL BEHAVIOR OF AS/3501-6
GRAPHITE/EPOXY MATERIAL - PHASE IV**

T. HO

R. A. SCHAPERY

VOUGHT CORPORATION ADVANCED TECHNOLOGY CENTER

P. O. BOX 225907

DALLAS, TEXAS 75265

FEBRUARY 1983

FINAL REPORT FOR PERIOD AUGUST 1981 - NOVEMBER 1982

Approved for public release; distribution unlimited

Prepared for:

Department of the Navy
Naval Air Systems Command
Washington, D.C. 20361

DTIC
OCT 7 1983

 **VOUGHT CORPORATION**
Advanced Technology Center

DTIC FILE COPY

83 09 23 018

UNCLASSIFIED

SECURITY CLASSIFICATION OF THIS PAGE (When Data Entered)

REPORT DOCUMENTATION PAGE		READ INSTRUCTIONS BEFORE COMPLETING FORM
1. REPORT NUMBER	2. GOVT ACCESSION NO.	3. RECIPIENT'S CATALOG NUMBER
	AD-A133331	
4. TITLE (and Subtitle)	5. TYPE OF REPORT & PERIOD COVERED	
THE EFFECT OF ENVIRONMENT ON THE MECHANICAL BEHAVIOR OF AS/3501-6 GRAPHITE/EPOXY MATERIAL - PHASE IV	FINAL REPORT AUGUST 1981-NOVEMBER 1982	
7. AUTHOR(s)	6. PERFORMING ORG. REPORT NUMBER	
T. HO R. A. SCHAPERY	R92000-3CR-9	
9. PERFORMING ORGANIZATION NAME AND ADDRESS	8. CONTRACT OR GRANT NUMBER(s)	
VOUGHT CORPORATION ADVANCED TECHNOLOGY CENTER P. O. BOX 225907 DALLAS, TEXAS 75265	N00019-81-C-0179	
11. CONTROLLING OFFICE NAME AND ADDRESS	10. PROGRAM ELEMENT, PROJECT, TASK AREA & WORK UNIT NUMBERS	
DEPARTMENT OF THE NAVY NAVAL AIR SYSTEMS COMMAND WASHINGTON, D.C. 20361		
14. MONITORING AGENCY NAME & ADDRESS (if different from Controlling Office)	12. REPORT DATE	
	FEBRUARY 1983	
	13. NUMBER OF PAGES	
	71	
	15. SECURITY CLASS. (of this report)	
	UNCLASSIFIED	
	15a. DECLASSIFICATION/DOWNGRADING SCHEDULE	
16. DISTRIBUTION STATEMENT (of this Report)		
APPROVED FOR PUBLIC RELEASE; DISTRIBUTION UNLIMITED		
17. DISTRIBUTION STATEMENT (of the abstract entered in Block 20, if different from Report)		
18. SUPPLEMENTARY NOTES		
19. KEY WORDS (Continue on reverse side if necessary and identify by block number)		
Composite, Viscoelasticity, Humidity, Temperature, Fatigue, Creep, Crack Propagation		
20. ABSTRACT (Continue on reverse side if necessary and identify by block number)		
The effect of temperature and moisture on the fatigue properties of AS/3501-6 composite was investigated. Micromechanics was used to relate the composite's compliance to the matrices' compliance. The stress state of the laminate was studied by using Tsai-Wu quadratic failure criterion through uniaxial specimen testings. Intralaminar cracks and delaminations were studied by testing $(+45/90_2)_s$ layup specimens. A laminate analysis method was used to evaluate the energy release rate of the $(+45/90_2)_s$ specimens. Results indicate that		

DD FORM 1473
1 JAN 73EDITION OF 1 NOV 65 IS OBSOLETE
S/N 0102-LF-014-6601

UNCLASSIFIED

SECURITY CLASSIFICATION OF THIS PAGE (When Data Entered)

UNCLASSIFIED

SECURITY CLASSIFICATION OF THIS PAGE (When Data Entered)

predicted critical strains are above those for which specimens begin to exhibit noticeable softening due to damage. To improve fatigue failure prediction behavior intraply microcracking must be accounted for in the theoretical model.

S-N 0102-LF-014 6601

UNCLASSIFIED

SECURITY CLASSIFICATION OF THIS PAGE (When Data Entered)

FOREWORD

This report is for Phase IV of the program entitled "The Effect of Environment on Mechanical Behavior of AS/3501-6 Graphite/Epoxy Material." The work was conducted at Vought Corporation Advanced Technology Center. This report covers all contract work in the period 3 August 1981 to 3 November 1982 and was sponsored by the Naval Air Systems Command under Contract Number N00019-81-C-0179.

Mr. M. Stander was the Navy Project Manager and Mr. R. C. Knight was the Vought Project Manager. Key technical personnel were Dr. T. Ho, Principal Investigator, and Dr. R. A. Schapery, Texas A&M University, Technical Consultant.



Accession For

NTIS GRA&I	<input checked="" type="checkbox"/>
NTIS Mon	<input type="checkbox"/>
Unannounced	<input type="checkbox"/>
Continuation	<input type="checkbox"/>

17

A

TABLE OF CONTENTS

<u>SECTION NO.</u>		PAGE
	FOREWORD	i
	LIST OF FIGURES	iii
	LIST OF TABLES	v
	LIST OF SYMBOLS	vi
1.0	INTRODUCTION	1
2.0	MICROMECHANICS	4
3.0	SPECIMEN FABRICATION AND CONDITIONING	16
4.0	STATIC TESTS AND ANALYSIS	23
	4.1 STATIC TESTS	23
	4.2 ANALYSIS	23
5.0	FATIGUE TESTS AND ANALYSIS	32
6.0	RESIDUAL STRENGTH TESTS AND DELAMINATION TESTS	46
7.0	ANALYSIS OF DAMAGE GROWTH AND FAILURES	57
	7.1 DAMAGE THEORY FOR LINEAR ELASTIC COMPOSITES	57
8.0	DISCUSSION AND CONCLUSIONS	69
9.0	REFERENCES	70

LIST OF FIGURES

<u>FIGURE</u>		<u>PAGE</u>
1.	Program Schedule	3
2.	The Relationship of Laminate Fatigue Compliance to Matrix Fatigue Compliance	5
3.	Fiber and Lamina Property Relationships (I)	9
4.	Fiber and Lamina Property Relationships (II)	10
5.	Laminate Compliance vs. Matrix Compliance	15
6.	Dimensions of Composite Panels	19
7.	Typical Test Specimens	20
8.	Location Delamination Defect	21
9.	Static Test Arrangement and Data Acquisition System	24
10.	Strength of static Specimens	25
11.	Modulus of Static Specimens	26
12.	Uniaxial Specimens Theoretical Strength Diagram	30
13.	A Radiographic Technique for Gr/Ep Specimens	31
14.	Mean Fatigue Strain Curve of $(\pm 45/90_2)_S$ Specimen at 75 ⁰ F/50% RH Environment	33
15.	Mean Fatigue Strain Curve of $(\pm 45/90_2)_S$ Specimen at 132 ⁰ F/50% RH Environment	34
16.	Mean Fatigue Strain Curve of $(\pm 45/90_2)_S$ Specimen at 132 ⁰ F/95% RH Environment	35
17.	Mean Fatigue Strain Curve of $(\pm 45/90_2)_S$ Specimen at 170 ⁰ F/50% RH Environment	36
18.	S-N Data of $(\pm 45/90_2)_S$ and $(90_2/\pm 45)_S$ Specimen	37
19.	Mean Fatigue Strain Curve of $(90_2/\pm 45)_S$ Specimen at 75 ⁰ F/50% RH	38
20.	Mean Fatigue Strain Curve of $(90_2/\pm 45)_S$ Specimens at 132 ⁰ F/95% RH	39
21.	Strain Amplitude of $(90_2/\pm 45)_S$ Specimen at 75 ⁰ F/50% RH	40
22.	Strain Amplitude of $(90_2/\pm 45)_S$ Specimens at 132 ⁰ F/95% RH	41
23.	Elastic Strain Ratio Translator (ESRT)	47
24.	Residual Strength Test Procedure	48
25.	Replication Prints of Edge Cracking for Specimens $(\pm 45/90_2)_S$ at 90% of Ultimate Load	51

LIST OF FIGURES

(Cont'd)

<u>FIGURE</u>		<u>PAGE</u>
26.	Typical Stress-Strain Curves at Various Stages of the Residual Strength Test	56
27.	End View of Tensile Specimen with a Pair of Delamination Cracks of Equal Depth.	61

LIST OF TABLES

<u>TABLE</u>		<u>PAGE</u>
1.	Formulas for Composite Moduli	6
2.	Parametric Dependence of Material Properties	8
3.	Longitudinal Modulus Properties for AS/3501-6	11
4.	Material Data	12
5.	Sensitivity Matrices	14
6.	Test Matrix	17
7.	Composite Panels for the Program	18
8.	The Layup Procedure and Cure Cycle for AS/3501-6	22
9.	Unidirectional Specimen Static Test Data Summary	27
10.	Failure Criterion Parameters	29
11.	Mechanical Properties of $(+45/90_2)_S$ Laminate in Phase III Program and Phase IV Program	42
12.	Test Data of AS-Type Fiber Composite	43
13.	Micromechanical Properties of AS-Type Fiber Composite	44
14.	Residual Strength Test Summary in 75°F/50% RH Environment	49
15.	Residual Strength Test Summary in 132°F/50% RH Environment	50
16.	Development of Cracks for $(+45/90_2)_S$ Specimens at 75°F/50% RH Environment	52
17.	Development of Cracks for $(+45/90_2)_S$ Specimens at 132°F/50% RH Environment	53
18.	Residual Strength Tests for $(+45/90_2)_S$ Delamination Specimens	55

LIST OF SYMBOLS

- A: Extensional stiffness matrix
A': Inverse representation of A
B: Bending and extensional stiffness matrix
B': Inverse representation of B
D: Bending stiffness matrix
D': Inverse representation of D
E: Young's modulus
 E_{LAM} : Young's modulus of laminate without delamination

E*: Young's modulus of laminate fully delaminated
F: Ultimate strength in failure criterion in the form of F_{xx} , F_{xy} ,
 F_{yy} , F_{ss} , F_x and F_y
 G_T : Shear modulus
M: Moment vector
N: Force vector
S: Shear strength
V: Volume in the forms of V_f or V_m
X: Longitudinal tensile direction or fiber direction
X': Longitudinal compressive direction
Y: Transverse tensile direction or perpendicular to fiber direction
Y': Transverse compressive direction

f: Fiber
h: Laminate thickness
k: Bulk constant
m: Matrix
s: Shear related quantity
x: Longitudinal direction
y: Transverse direction

: Normal strain quantity
: Shear strain quantity
: Curvature quantities
: Poisson's ratio

1.0 INTRODUCTION

Wide usage of advanced composite materials in future aerospace systems is projected to become a reality over the next few years. A V/STOL fighter aircraft is one of several Navy articles expected to be increasingly dependent on composite materials for primary and secondary structural components.

Presently, the response of advanced composite materials to arbitrary load and environments is known to have a significant adverse effect on the materials performance. The materials response in severe environments and related fatigue lifetime prediction methods are presently insufficient. It is believed this composites research program assists in resolving this deficiency in the technology base.

The overall objectives of this research program are:

- o To ascertain if the mechanical response of AS/3501-6 graphite/epoxy composite material, subject to various time, temperature and moisture effects, can be characterized using traditional viscoelastic shift factors, and to formulate a master curve of material property dependence on time, temperature and humidity if possible.
- o To ascertain the feasibility of predicting fatigue failure of a composite material by accounting for the linear viscoelastic behavior of the resin in various temperature and humidity environments.
- o To determine if a specific thermal conditioning environment can be directly substituted for a specific moisture conditioning environment, over a prescribed temperature vs. humidity range for AS/3501-6 graphite/epoxy material, and obtain an equivalent moisture effect on mechanical and fatigue properties. If this can be shown, a substantial cost and time savings in moisture conditioning of the test specimen can be achieved and possibly extended to other composite specimens.

Through the research of the Phase I program¹ the first and third objectives previously mentioned were accomplished. Thus, linear viscoelasticity is an appropriate method to characterize the composite's response with respect to time, temperature and humidity. A definitive equivalence relationship between one environment and another is not feasible in the sense that each temperature/humidity condition's effect on the materials mechanical response is unique in itself.

The research objective of this Phase IV program was to continue the Phase II and Phase III effort to accomplish the second objective, i.e., to predict the fatigue failure of composite material by accounting for its viscoelastic behavior in various temperature and humidity environments.

The basic Phase IV program scope was increased to evaluate the edge cracking and delamination of the $(+45/90_2)_5$ layup to supplement the fatigue data obtained from the previous Phases II² and III.³ This added scope entailed the residual strength tests and delamination tests on graphite/epoxy coupons. Since the fatigue analysis requires that the state of stress of the lamina be known, off-axis specimen tests were conducted.

The Phase IV program schedule is shown in Figure 1.

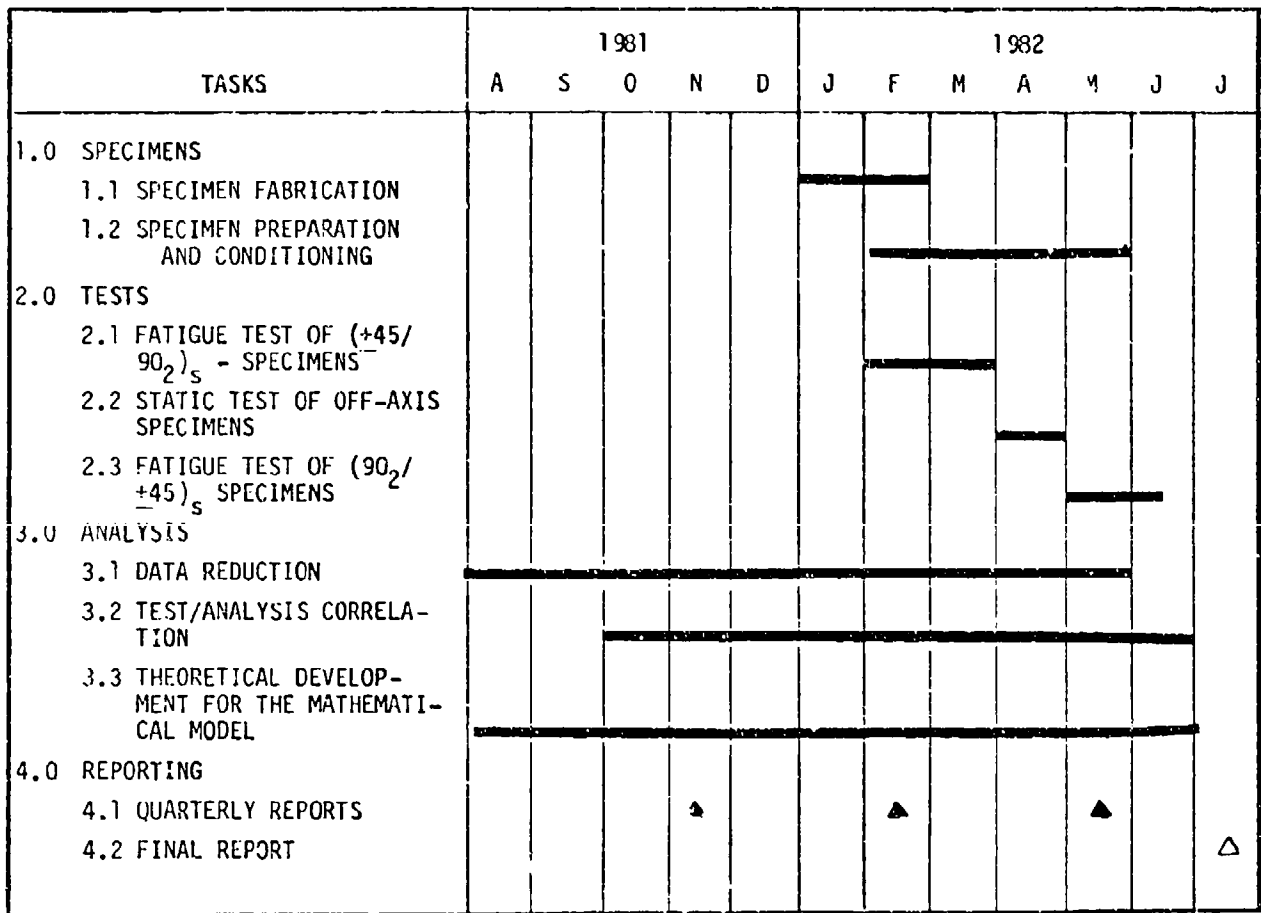


FIGURE 1 PROGRAM SCHEDULE

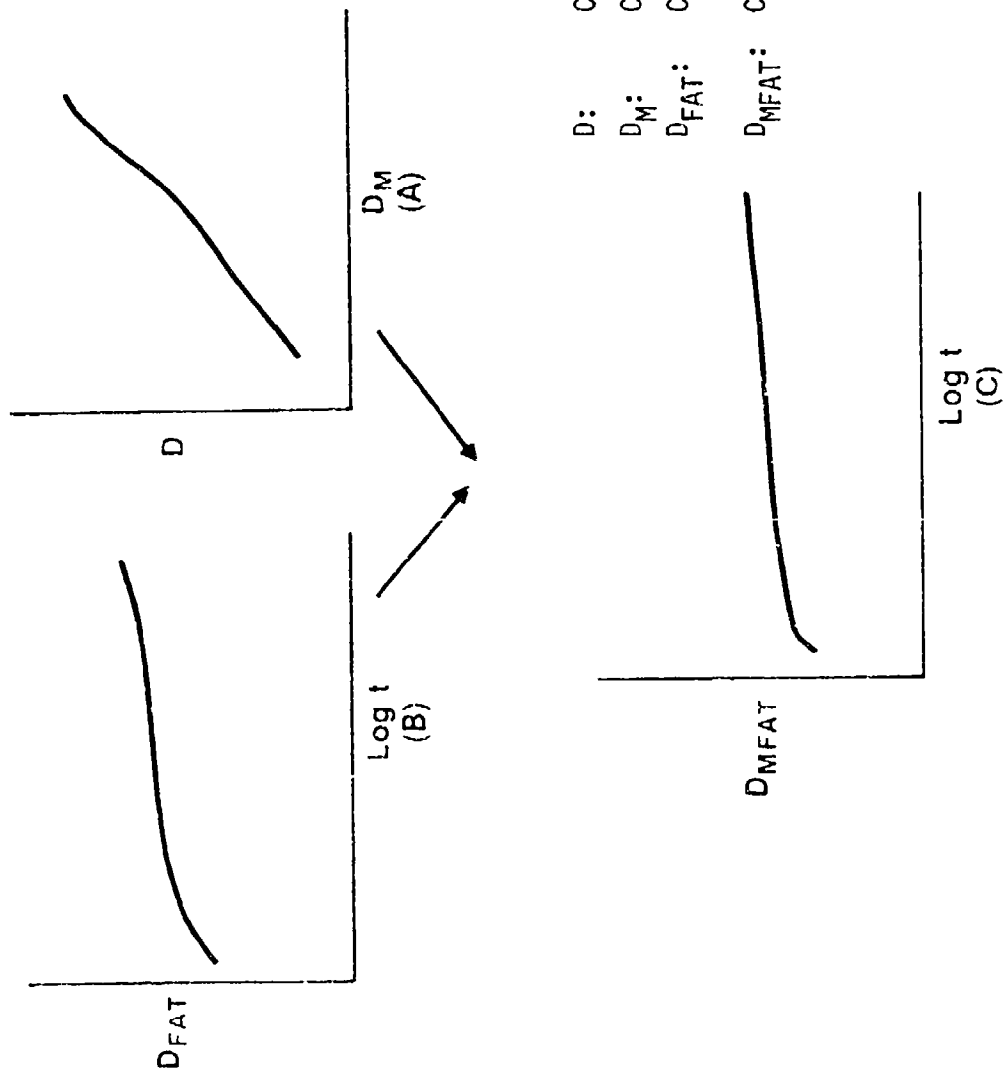
2.0 MICROMECHANICS

Results from Phase II and Phase III programs indicated that, for the matrix dominated laminate such as the $(+45^0/90^0)_2$ layup, composite fatigue characteristics can be interpreted better by relating to the matrix through micromechanics as illustrated in Figure 2. In this approach, laminate characteristics are first related to the lamina properties which, in turn, are related to the matrix properties. Since lamina properties are needed to relate the laminate to the matrix, quadratic tensor polynomial criteria is adapted to quantify the general stress state of the laminate.

In fatigue analysis, the edge delamination type failure mode is believed to be involved in the fatigue failure. The separation of delamination failure mode data from normal matrix damage degradation data is needed before the analysis procedure in Figure 2 can be used properly.

The Tsai-Hahn micromechanics relationships⁴ have been incorporated into the LAMINATE ANALYSIS computer program. The formulas for the micromechanic relationships are shown in Table 1. These relationships originated from Hashin's composite cylinder assemblage (CCA) model.⁵ Especially, the value of transverse shear modulus, G_y , and transverse Young's modulus, E_y , are upper bounds of the CCA model. Nevertheless, the Tsai-Hahn relationships are simple enough for engineering applications.

The use of the Tsai-Hahn relationships for advanced composites is not straightforward due to the unknown nature of both its fiber and matrix properties, especially in their in-situ state. On the basis of measured modulus values of unidirectional graphite/epoxy composite, five anisotropic fiber properties (E_{1f} , E_{2f} , G_{12f} , G_{23f} , ν_{12f}) and two isotropic matrix properties (E_m , ν_m) can be recovered without direct measurement of each constituent's properties, which are difficult to obtain with current test techniques. The procedure for finding these seven material properties is a combination of matrix property assumptions and parametric sensitivity relationships. Although this is a cumbersome approach to obtain the material properties, it is an easier task than trying the analytical conversion of the relationships in Table 1 and the corresponding expensive test program.



D: COMPLIANCE OF COMPOSITE
 D_M : COMPLIANCE OF MATRIX
 D_{FAT} : COMPLIANCE OF COMPOSITE DURING FATIGUE
 D_{MFAT} : COMPLIANCE OF MATRIX DURING FATIGUE

FIGURE 2. THE RELATIONSHIP OF LAMINATE FATIGUE COMPLIANCE TO MATRIX FATIGUE COMPLIANCE

TABLE 1 FORMULAS FOR COMPOSITE MODULI

$$P = \frac{1}{V_f + \eta V_m} (V_f P_f + \eta V_m P_m)$$

ENGINEERING CONSTANT	P	P _f	P _m	η
E _x	E _x	E _f	E _m	1
ν _x	ν _x	ν _f	ν _m	1
E _s	$\frac{1}{E_s}$	$\frac{1}{G_f}$	$\frac{1}{G_m}$	η _s
k _y	$\frac{1}{k_y}$	$\frac{1}{k_{fy}}$	$\frac{1}{k_m}$	η _k
G _y	$\frac{1}{G_y}$	$\frac{1}{G_{fy}}$	$\frac{1}{G_m}$	η _G

where:

$$\eta_s = \frac{1}{2} \left(1 + \frac{G_m}{G_f} \right)$$

$$\eta_k = \frac{1}{2(1-\nu_m)} \left(1 + \frac{G_m}{k_{fy}} \right)$$

$$\eta_G = \frac{1}{4(1-\nu_m)} \left(3 - 4\nu_m + \frac{G_m}{G_{fy}} \right)$$

$$M = 1 + \frac{4k_y \nu_x^2}{E_x}$$

$$E_y = \frac{4k_y G_y}{k_y + M G_y}$$

- s = shear
- k = bulk modulus
- η = numerical constant(s)
- x = fiber direction
- y = transverse direction

A sensitivity study was conducted to specify the different combinations of the seven material properties most sensitive to the known unidirectional data. The unidirectional stiffness (Q_{ij}) properties of a lamina and/or general laminate can be represented by the parametric forms shown in Table 2 where fiber volume V_f is included for analysis. The Poisson's ratio of the matrix material is assumed to be 0.35 in all of these studies. The sensitivity relations of Q_{ij} are obtained

$$\begin{aligned}
 \frac{\Delta Q_{ij}}{Q_{ij}} = & \frac{\partial \ln Q_{ij}}{\partial \ln E_{1f}} \frac{\Delta E_{1f}}{E_{1f}} + \frac{\partial \ln Q_{ij}}{\partial \ln E_{2f}} \frac{\Delta E_{2f}}{E_{2f}} + \frac{\partial \ln Q_{ij}}{\partial \ln G_{23f}} \frac{\Delta G_{23f}}{G_{23f}} \\
 & + \frac{\partial \ln Q_{ij}}{\partial \ln G_{12f}} \frac{\Delta G_{12f}}{G_{12f}} + \frac{\partial \ln Q_{ij}}{\partial \ln \nu_{12f}} \frac{\Delta \nu_{12f}}{\nu_{12f}} + \frac{\partial \ln Q_{ij}}{\partial \ln E_m} \frac{\Delta E_m}{E_m} \\
 & + \frac{\partial \ln Q_{ij}}{\partial \ln V_f} \frac{\Delta V_f}{V_f}
 \end{aligned} \tag{1}$$

by taking the differentials in the Q_{ij} function. Equation (1) can then be used to evaluate the percent change of Q_{ij} due to percent change of the parameters in Table 2.

Alternately, by assuming $E_m = 0.66$ msi, functional dependence of the unidirectional properties on each of their dominant parameters are obtained using the LAMINATE ANALYSIS computer routine. Results are shown in Figures 3 and 4. Axial modulus E_{11} of different graphite/epoxy layups are obtained from test results in References 1, 2, and 6 and are shown in Table 3 for both room temperature environment and a 170°F/50% R.H. environment. With the information from Figures 3 and 4 and Table 3, the fiber and matrix properties were derived, and are shown in Table 4. From Equation (1) and Table 4, the sensitivity matrix for unidirectional lamina and $(\pm 45/90_2)_S$

TABLE 2 PARAMETRIC DEPENDENCE OF MATERIAL PROPERTIES

LAMINA PROPERTIES:

$$E_{11} = \hat{E}_{11}(E_{1f}, E_m, V_f)$$

$$E_{22} = \hat{E}_{22}(E_{2f}, G_{23f}, E_m, V_f, \nu_{12f}, E_{1f})$$

$$G_{12} = \hat{G}_{12}(G_{12f}, E_m, V_f)$$

$$\nu_{12} = \hat{\nu}_{12}(\nu_{12f}, E_m, V_f)$$

$$G_{23} = \hat{G}_{23}(G_{23f}, E_m, V_f)$$

LAMINATE PROPERTIES:

$$Q_{ij} = \hat{Q}_{ij}(E_{1f}, E_{2f}, G_{23f}, G_{12f}, \nu_{12f}, E_m, V_f)$$

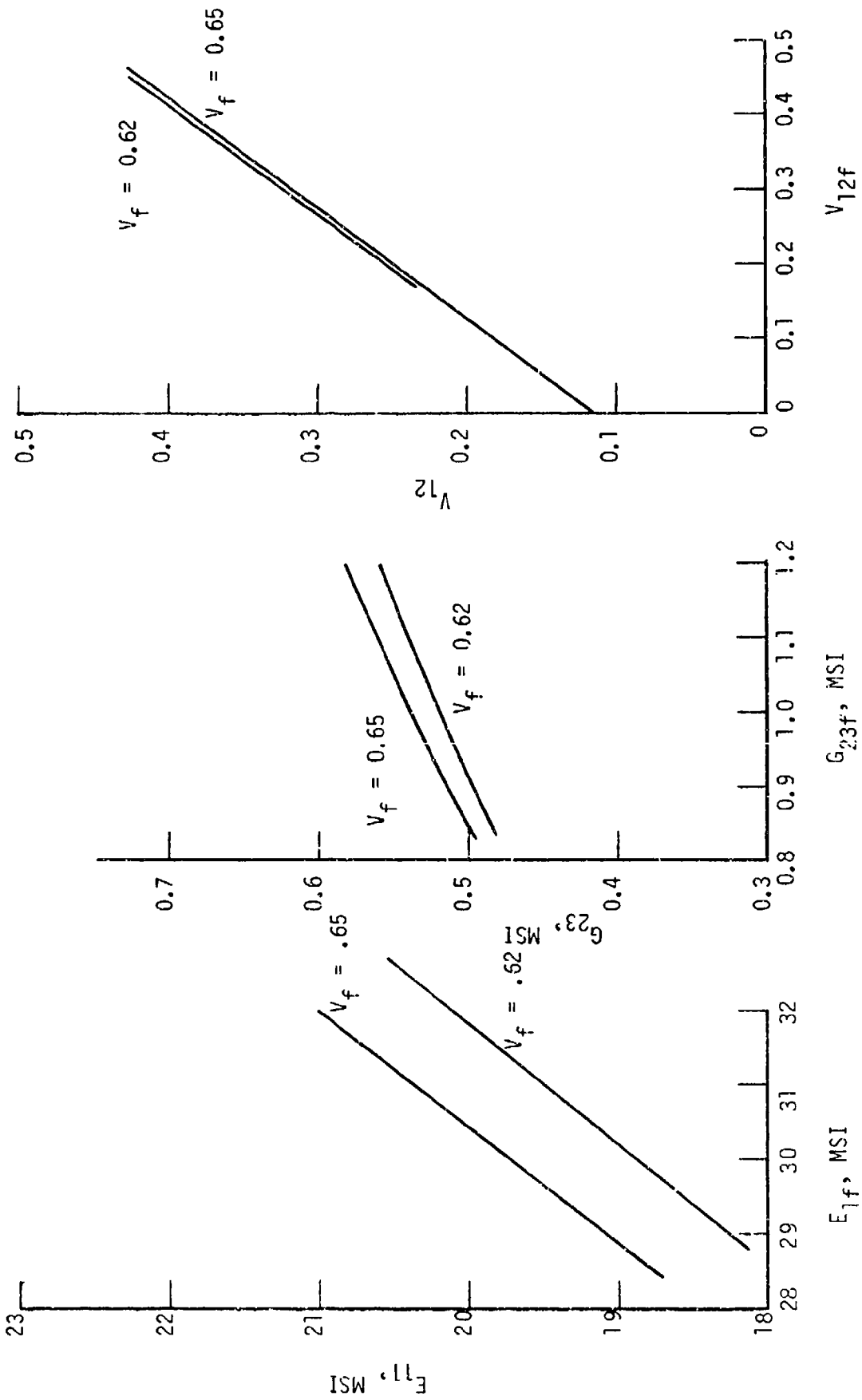


FIGURE 3 FIBER AND LAMINA PROPERTY RELATIONSHIPS (1)

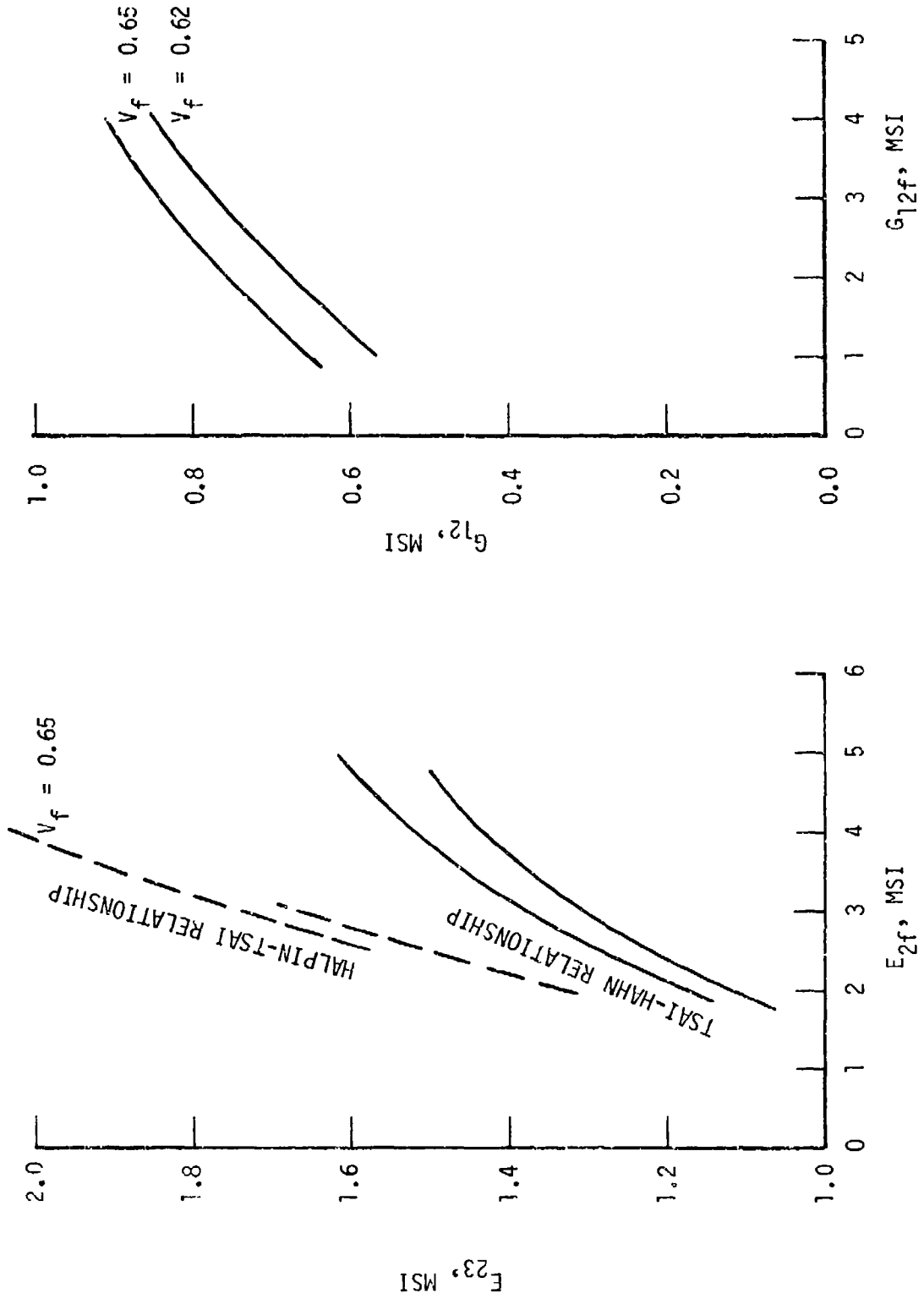


FIGURE 4 FIBER AND LAMINA PROPERTY RELATIONSHIPS (II)

TABLE 3 LONGITUDINAL MODULUS PROPERTIES FOR AS/3501-6

ENVIRONMENTS	SPECIMEN LAYUP	RESULTS FROM TSAI-HAHN RELATIONS (MSI)	EXPERIMENTAL RESULTS (MSI)
75°F/50% R.H.	(0) ₈	18.82	18.95
	(+45) _{2s}	2.81	2.80
	(90) ₂₀	1.54	1.54
	(+45/90) _{2s}	3.36	2.82
	(0/+45/90) _s	7.44	7.20
170°F/50% R.H.	(0) ₈	18.80	18.95
	(+45) _{2s}	2.36	2.10
	(90) ₂₀	1.33	1.33
	(+45/90) _{2s}	3.14	2.66
	(0/+45/90) _s	7.25	7.06

TABLE 4 MATERIAL DATA

CONSTITUENTS' DATA FOR Gr/Ep

$$E_{1f} = 28.6 \text{ MSI}$$

$$E_{2f} = 4.2 \text{ MSI}$$

$$G_{23f} = 0.89 \text{ MSI}$$

$$G_{12f} = 2.50 \text{ MSI}$$

$$\nu_{12f} = 0.32$$

$$\nu_f = 0.65$$

$$E_m = 0.66 \text{ MSI}$$

$$\nu_m = 0.35$$

COMPOSITE DATA FROM MICROMECHANICS

$$E_1 = 18.82 \text{ MSI}$$

$$E_2 = 1.54 \text{ MSI}$$

$$G_{12} = 0.805 \text{ MSI}$$

$$G_{23} = 0.512 \text{ MSI}$$

$$\nu_{12} = 0.33$$

laminates as shown in Table 5 may be calculated. The significant information obtained from the sensitivity matrix assuming that the matrix properties are fixed is:

1. Fiber volume fraction is the most dominant parameter affecting material property change of either a lamina or laminate (Table 5).
2. Unidirectional properties E_{11} , E_{22} , G_{12} , G_{23} and ν_{12} are also strongly influenced by fiber properties E_{1f} , E_{2f} , G_{12f} , G_{23f} , and ν_{12f} respectively.

These results are helpful in adjusting values in Table 4 to meet different graphite/epoxy test results. With the LAMINATE ANALYSIS computer program, the effect of matrix modulus on laminate E_{11} property can be evaluated. The result is shown in Figure 5 where the compliance curves, instead of modulus, are compiled. These curves are important in analyzing both fatigue strength and fatigue failure data according to the compliance relationship in Figure 2. There is one question in correlating the LAMINATE ANALYSIS results to the real test data. In comparing the laminate data in Table 3, especially those from complicated lay-ups, values of laminate E_{11} obtained from the LAMINATE ANALYSIS program are higher than those obtained from tests. This situation has been analyzed by Arenburg⁷ who attributes at least some of the difference to transverse shear property effects as defined in his finite element analysis. There are more discussions on this in Section 4.0.

TABLE 5 SENSITIVITY MATRICES

SENSITIVITY MATRIX FOR UNIDIRECTIONAL LAMINA

	$\frac{\Delta E_{1f}}{E_{1f}}$	$\frac{\Delta E_{2f}}{E_{2f}}$	$\frac{\Delta G_{23f}}{G_{23f}}$	$\frac{\Delta G_{12f}}{G_{12f}}$	$\frac{\Delta \nu_{12f}}{\nu_{12f}}$	$\frac{\Delta E_m}{E_m}$	$\frac{\Delta \nu_f}{\nu_f}$
$\frac{\Delta E_{11}}{E_{11}}$	0.988	0	0	0	0	0.012	0.967
$\frac{\Delta E_{22}}{E_{22}}$	0	0.292	-0.026	0	0	0.624	1.603
$\frac{\Delta G_{23}}{G_{23}}$	0	0	0.43	0	0	0.447	0.820
$\frac{\Delta G_{12}}{G_{12}}$	0	0	0	0.273	0	0.615	1.69
$\frac{\Delta \nu_{12}}{\nu_{12}}$	0	0	0	0	0.606	0	0

SENSITIVITY MATRIX FOR $(\pm 45/90)_2$ LAMINATE

	$\frac{\Delta E_{1f}}{E_{1f}}$	$\frac{\Delta E_{2f}}{E_{2f}}$	$\frac{\Delta G_{23f}}{G_{23f}}$	$\frac{\Delta G_{12f}}{G_{12f}}$	$\frac{\Delta \nu_{12f}}{\nu_{12f}}$	$\frac{\Delta E_m}{E_m}$	$\frac{\Delta \nu_f}{\nu_f}$
$\frac{\Delta E_{11}}{E_{11}}$	0.554	0.083	-0.012	0.042	0	0.281	1.256
$\frac{\Delta E_{22}}{E_{22}}$	0.355	0.039	0.003	0.039	0.003	0.079	1.065
$\frac{\Delta G_{23}}{G_{23}}$	-	-	-	-	-	-	-
$\frac{\Delta G_{12}}{G_{12}}$	0.824	0.011	0	0.046	-0.011	0.117	1.098
$\frac{\Delta \nu_{12}}{\nu_{12}}$	0.050	0.050	0.050	-0.050	0.099	0	0.050

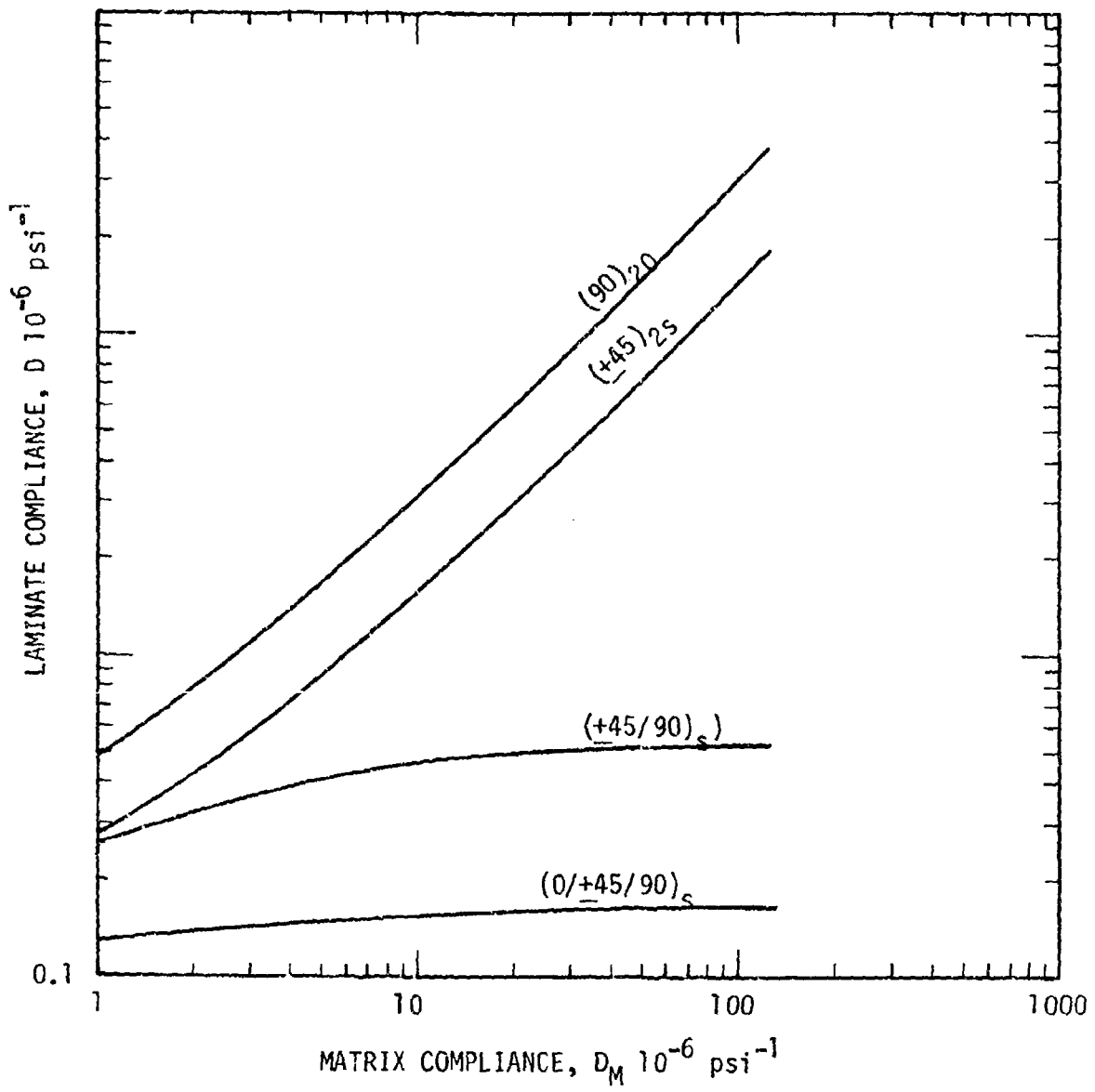


FIGURE 5 LAMINATE COMPLIANCE VS. MATRIX COMPLIANCE

3.0 SPECIMEN FABRICATION AND CONDITIONING

After reviewing the fatigue data of the AS/3501-6 graphite/epoxy specimens,^{2,3} it seemed important to study the influence of matrix degradation on the edge delamination failure mode in the fatigue process. The test program was defined as shown in Table 6. The residual strength tests and delamination tests are designed to evaluate the edge cracking phenomenon.

Hercules AS1/3501-6 graphite/epoxy prepreg tape was used to prepare the specimens. A total of 232 specimens to be tested according to test matrix, Table 6, were obtained from fourteen panels of different sizes as shown in Table 7 and Figure 6. The various sizes of the panels resulted from the ply lay-up variation, defect insertions and the number of specimens required. Typical specimen dimensions are 7" long by 0.75" wide as shown in Figure 7. The delamination specimens have brass shim inserts (0.001" thick) at the edges as shown in Figure 8 to simulate the edge cracks. Typical layup procedures and cure cycles are shown in Table 8.

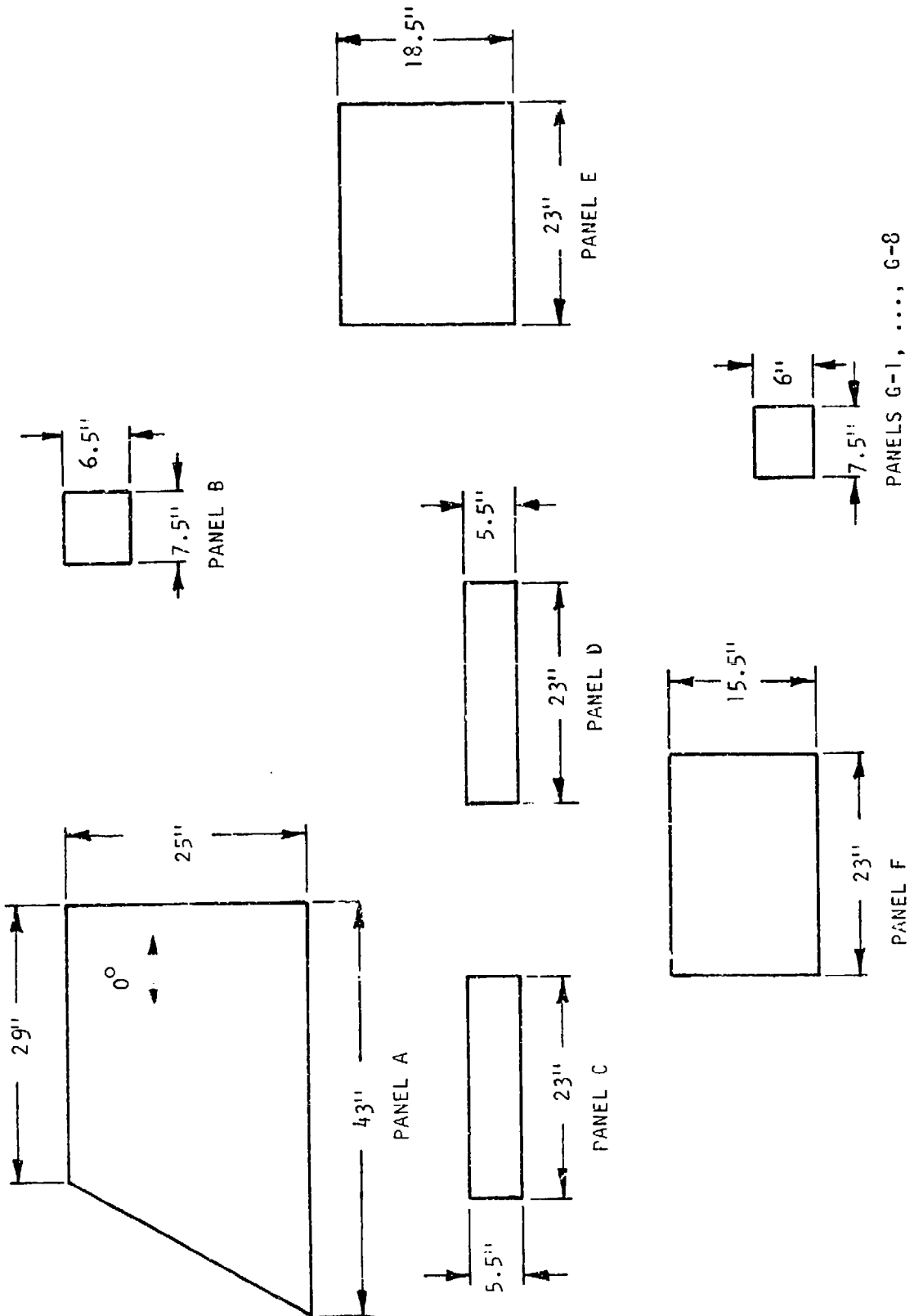
For moisture absorption, steel chambers enclosed in a forced air Blue-M oven were used to environmentally condition the specimens to the desired moisture levels. A saturated aqueous solution of sodium bromide (NaBr) in contact with a solid phase of the salt at 170°F was used to generate the 50% relative humidity level. Sodium fluoride (NaF) was used to generate the 95% relative humidity level. Approximately, fifteen days of conditioning was required for the eight-ply specimens and eighty-five days for the twenty-ply specimens. The moisture distribution inside the specimen should reach a reasonably uniform state after the above mentioned conditioning period. All specimen end tabs were protected with aluminum backing tape wrapping and EA934 coating to prevent moisture ingress during the environmental conditioning process.

TABLE 6 TEST MATRIX

TEST	TYPE OF TEST	TEST ENVIRONMENT (°F/% RH)	NUMBER OF SPECIMENS									
			(0) 8	(15) 20	(30) 20	(45) 20	(60) 20	(90) 20	(+45/90) 2 s	(90 ₂ /+45) s		
A	STATIC	75/50		3	3	3	3	3	3	3	2	2
		75/95		3	3	3	3	3	3	3		
		132/50		3	3	3	3	3	3	3	2	
		132/95		3	3	3	3	3	3	3		2
		170/50	3	3	3	3	3	3	3	3	2	
		75/DRY	3	3	3	3	3	3	3	3	2	
B	RESIDUAL STRENGTH TEST	75/50									24	
		132/50									24	
C	FATIGUE TEST	75/50									6	18
		132/95										18
D	DELAMINATION	75/50									16	
		170/50									16	

TABLE 7 COMPOSITE PANELS FOR THE PROGRAM

PANEL	SPECIMEN LAY-UP	NO. OF SPECIMENS FABRICATED	SPECIAL FEATURE OF THE SPECIMEN
A	(15) ₂₀	18	
	(30) ₂₀	18	
	(60) ₂₀	18	
B	(0) ₈	6	
C	(45) ₂₀	18	
D	(90) ₂₀	18	
E	(<u>+45/90</u>) ₂ _s	62	
F	(90 ₂ / <u>+45</u>) _s	42	
G-1	(<u>+45/90</u>) ₂ _s	4	WITH 0.02" INSERTS IN THE MIDDLE LEVEL
G-2	(<u>+45/90</u>) ₂ _s	4	
G-3	(<u>+45/90</u>) ₂ _s	4	WITH 0.04" INSERTS IN THE MIDDLE LEVEL
G-4	(<u>+45/90</u>) ₂ _s	4	
G-5	(<u>+45/90</u>) ₂ _s	4	WITH 0.02" INSERTS IN THE QUARTER THICKNESS LEVEL
G-6	(<u>+45/90</u>) ₂ _s	4	
G-7	(<u>+45/90</u>) ₂ _s	4	WITH 0.04" INSERTS IN THE QUARTER THICKNESS LEVEL
G-8	(<u>+45/90</u>) ₂ _s	4	



PANELS G-1, ..., G-8

FIGURE 6 DIMENSIONS OF COMPOSITE PANELS

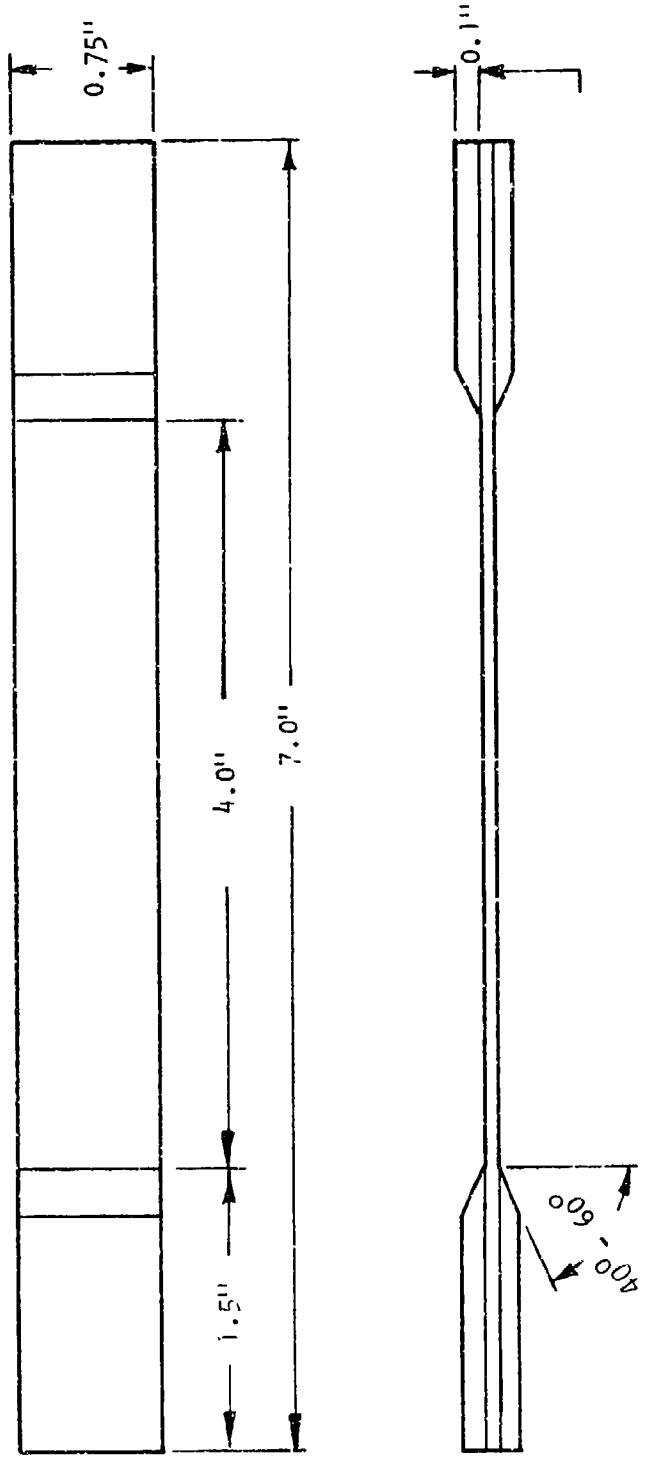
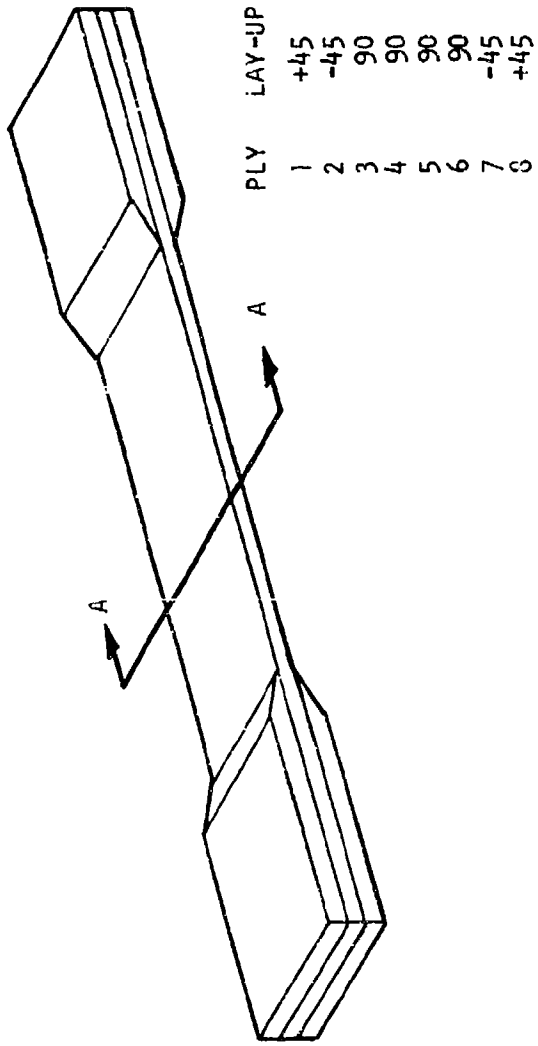


FIGURE 7 TYPICAL TEST SPECIMENS



BRASS SHIM
(TYPICAL)

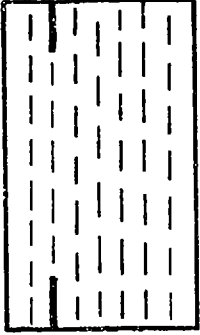
1 PLY



0.02" BRASS SHIM
FOR PANELS G1, G2



0.04" BRASS SHIM
FOR PANELS G3, G4



0.02" BRASS SHIM
FOR PANELS G5, G6



0.04" BRASS SHIM
FOR PANELS G7, G8

VIEW A-A

FIGURE 8 LOCATION OF DELAMINATION DEFECT

TABLE 3 THE LAYUP PROCEDURE AND CURE CYCLE FOR AS/3501-6

<p>The layup procedure was:</p> <ul style="list-style-type: none"> o Clean all tooling o Apply a mold release agent to the tooling and caul plate o Cover both surfaces of the layup with TX-1040 o Position the layup on the tool o Apply the cork dam and 6 bleeder plies o Cover the layup with nylon film o Cover the layup with two plies of fiberglass breather cloth o install the layup in a vacuum bag and place in an autoclave 	<p>The cure cycle was:</p> <ul style="list-style-type: none"> o Apply 25" Hg minimum vacuum o Apply 10 psi autoclave pressure o Heat to $350 \pm 5^{\circ}\text{F}$ (5-10^oF/min rate) o Apply 90 + 5 psi autoclave pressure when the panel reaches $275 \pm 50^{\circ}\text{F}$ (DO NOT VENT) o Maintain the laminate at $350 \pm 5^{\circ}\text{F}$ for 120 ± 5 minutes o Cool slowly to below 150°F (Cool no faster than 5°F per minute - Cool down should take approximately 45 minutes)
---	--

4.0 STATIC TESTS AND ANALYSIS

4.1 STATIC TESTS

Off-axis static tests were conducted according to the test matrix of Table 6. The six types of unidirectional specimens for off-axis tests are $(0^\circ)_g$, $(15^\circ)_{20}$, $(30^\circ)_{20}$, $(45^\circ)_{20}$, $(60^\circ)_{20}$, and $(90^\circ)_{20}$. Some static tests were also conducted on $(\pm 45^\circ / 90^\circ)_s$ and $(90^\circ / \pm 45^\circ)_s$ laminates and the data used to verify the quadratic tensor failure criterion.

Tests were performed using a Shorewestern environmental test machine as illustrated in Figure 9. Six temperature and humidity test environments were: 75°F/dry, 75°F/50% RH, 75°F/95% RH, 132°F/50% RH, 132°F/95% RH, and 170°F/50% RH. Extensometers were used to measure the strain at the two-inch gage section of the test specimen. For selected 75°F/dry environment tests, strain gages were also used in conjunction with the extensometers in order to verify the calibration of the extensometer system.

4.2 ANALYSIS

Test data are shown in Figure 10 for strength and Figure 11 for modulus. The best fit of lower and upper bounds for the test data are also drawn in the two figures together with the corresponding classical laminate analysis (CLA) comparison data to be explained below. The Poisson's ratio is 0.32 based on the $(0)_g$ specimen test at 75°F/dry environment with strain gages. Tabulated values of the upper and lower bounds in Figures 10 and 11 for various angles are shown in Table 9. The shear modulus G_{12} can be obtained by the following relationship:

$$G_{12} = \frac{2\nu_{12}}{E_{11}} + \frac{1}{\sin^2\theta \cos^2\theta} \left(\frac{1}{E'_{11}} - \frac{\cos^4\theta}{E_{11}} - \frac{\sin^4\theta}{E_{22}} \right) \quad (2)$$

where E_{11} is the longitudinal modulus, E_{22} is the transverse modulus and E'_{11} is the axial modulus of the off-axis specimen. Each off-axis specimen has a calculated G_{12} -value and the average G_{12} is 0.752 msi as derived

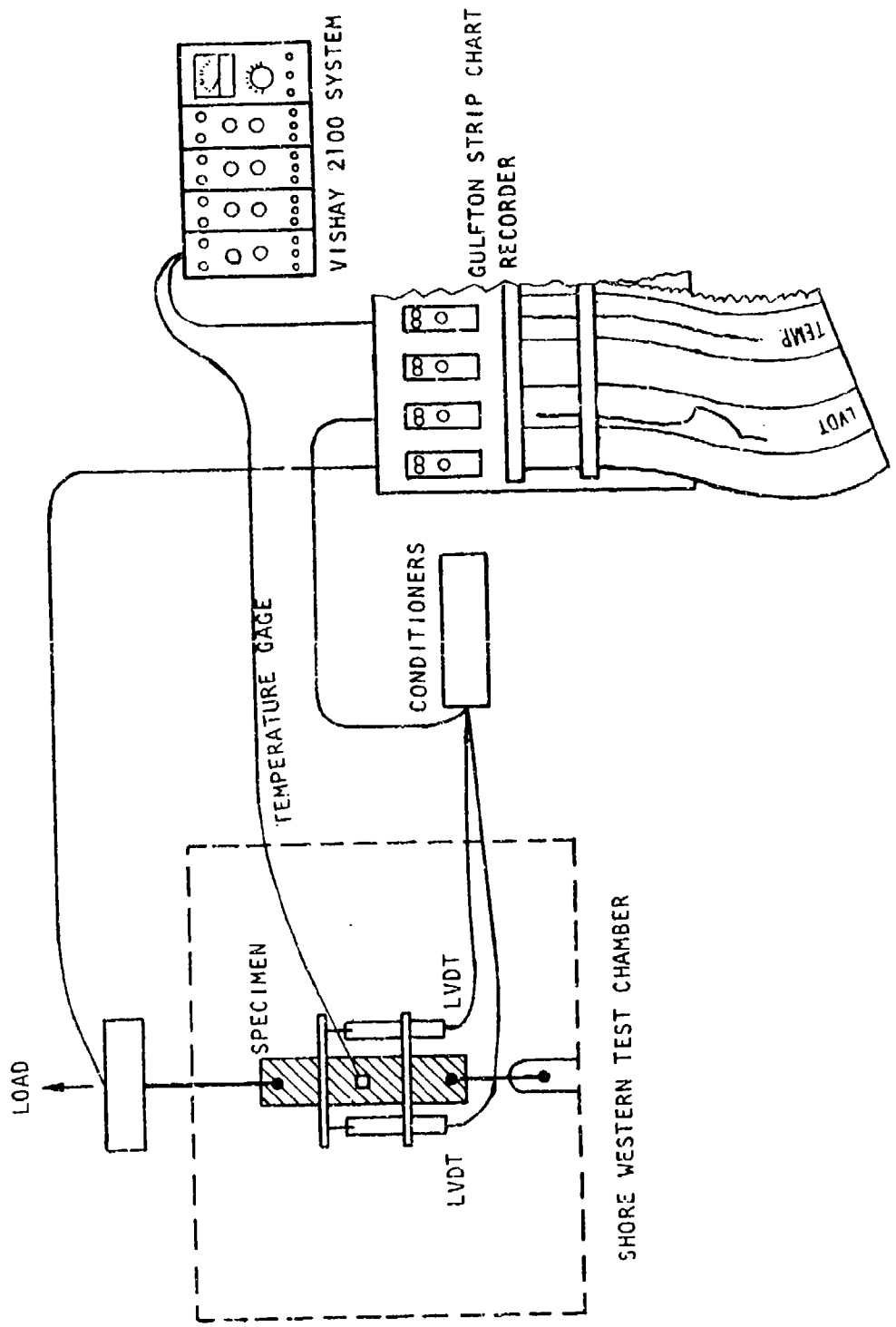


FIGURE 9. STATIC TEST ARRANGEMENT AND DATA ACQUISITION SYSTEM

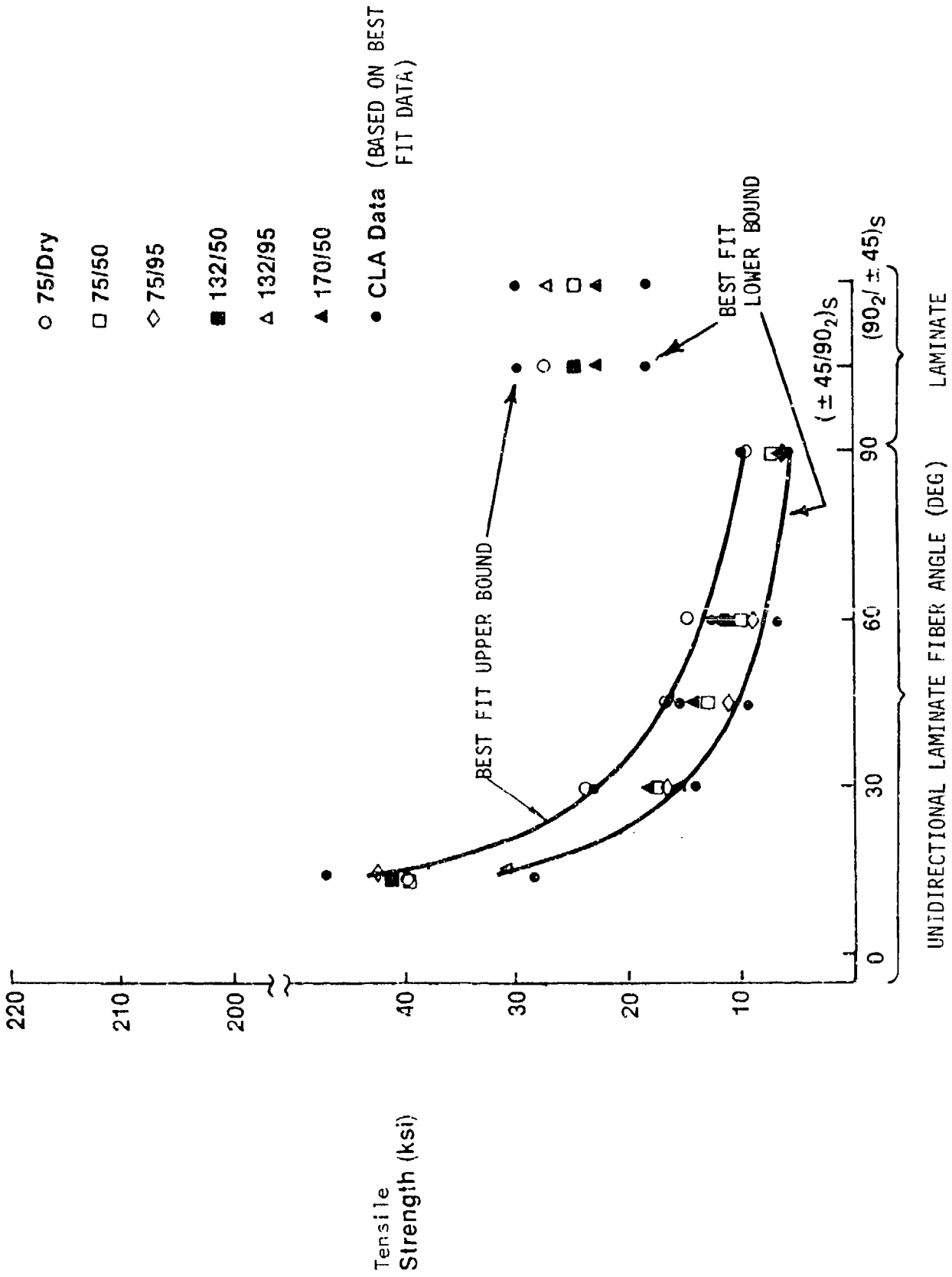


FIGURE 10 STRENGTH OF STATIC SPECIMENS

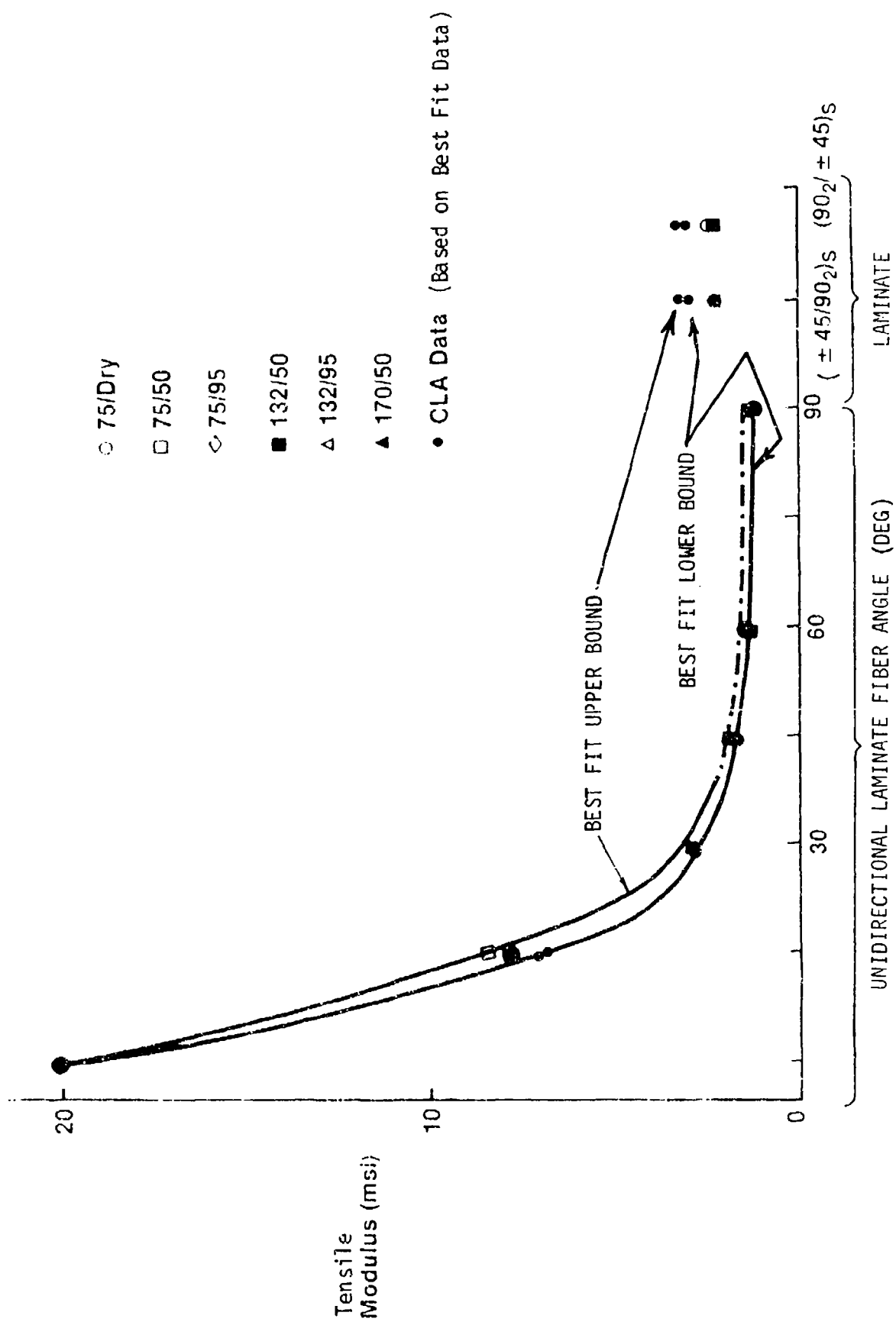


FIGURE 11 MODULUS OF STATIC SPECIMENS

TABLE 9 UNIDIRECTIONAL SPECIMEN STATIC TEST DATA SUMMARY

STRENGTH (msi)	(0) ₈	(15) ₂₀	(30) ₂₀	(45) ₂₀	(60) ₂₀	(90) ₂₀
UPPER BOUND	0.216	0.0415	0.0224	0.0164	0.0130	0.010
LOWER BOUND	0.205	0.0315	0.0151	0.0104	0.0078	0.006
MODULUS (msi)	(0) ₈	(15) ₂₀	(30) ₂₀	(45) ₂₀	(50) ₂₀	(90) ₂₀
UPPER BOUND	20.25	8.6	3.1	1.9	1.5	1.4
LOWER BOUND	20.25	7.1	2.7	1.6	1.3	1.2

from the upper bound test data and 0.62 msi from the lower bound. From the calculated average G_{12} value, and Equation (2), the theoretical modulus of the off-axis angle specimen is obtained. These theoretical modulus are shown in Figure 11. The test value and theoretical value show a favorable comparison. The theoretical values are used later to interpret the fracture energy and fatigue data.

The strength data in Figure 10 were used to evaluate the parameters of the Tsai-Wu quadratic failure criterion:

$$F_{xx} \sigma_x^2 + F_{xy} \sigma_x \sigma_y + F_{yy} \sigma_y^2 + F_{ss} \sigma_s^2 + F_x \sigma_x + F_y \sigma_y = 1 \quad (3)$$

where x is the longitudinal direction and y is the transverse direction. Since no compression or bi-axial tests were conducted, compression and shear data from Tsai-Hahn⁴ was used. By using the upper bound values and lower bound values from Figure 10, parameters in Equation (3) can be derived. Calculations and results are shown in Table 10. The theoretical strength diagram from the Tsai-Wu criterion is shown in Figure 12. The theoretical values (CLA) are also shown in Figure 10 to compare with test data. The static strength values of the $(+45/90_2)_s$ fall within the theoretical range for $(+45/90_2)_s$ specimens. The Tsai-Wu criterion can be reasonably used for fatigue failure analysis if the residual strength is not affected after fatigue cycling.

To study the failed specimen, a radiographic technique was developed for inspection of graphite/epoxy specimens. The delaminations present in the specimens could not be detected initially by conventional X-ray methods. A radiographic-opaque solution (ZnI_2) was developed and applied to the edges of each of the failed specimens with cotton swabs. After a fifteen minute "dwell time" had elapsed, the specimens were re-exposed with the x-ray instrument settings remaining the same. The radiograph from the second exposure (with solution applied) enabled complete detection of the delaminated areas of each specimen with excellent detail as shown in Figure 13. Massive delaminations in the outside 90° layers for $(90_2/+45)_s$ type specimens were observed all over the length of the specimen. Delaminations of 90° layers in the $(+45/90_2)_s$ are more confined to the edges.

TABLE 10 FAILURE CRITERION PARAMETERS

STRENGTH (msi)	X	X'	Y	Y'	S	
UPPER BOUND	0.216	0.216	0.010	0.030	0.0135	
LOWER BOUND	0.205	0.205	0.006	0.018	0.0081	
TSAI-WU QUADRATIC FAILURE CRITERION						
	F_{xx} (msi ⁻²)	F_{xy} (msi ⁻²)	F_{yy} (msi ⁻²)	F_{ss} (msi ⁻²)	F_x (msi ⁻¹)	F_y (msi ⁻¹)
UPPER BOUND	21.43	-133.6	3333	5489	0	66.7
LOWER BOUND	23.80	-234.7	9259	15242	0	111.1
<p>X : LONGITUDINAL TENSILE STRENGTH X' : LONGITUDINAL COMPRESSIVE STRENGTH Y : TRANSVERSE TENSILE STRENGTH Y' : TRANSVERSE COMPRESSIVE STRENGTH S : SHEAR STRENGTH</p> $F_{xx} = \frac{1}{xx^T}, F_{yy} = \frac{1}{yy^T}, F_{xy} = -1/2 \sqrt{F_{xx} F_{yy}}$ $F_{ss} = \frac{1}{s^2}, F_x = \frac{1}{s} - \frac{1}{x^T}, F_y = \frac{1}{y} - \frac{1}{y^T}$						

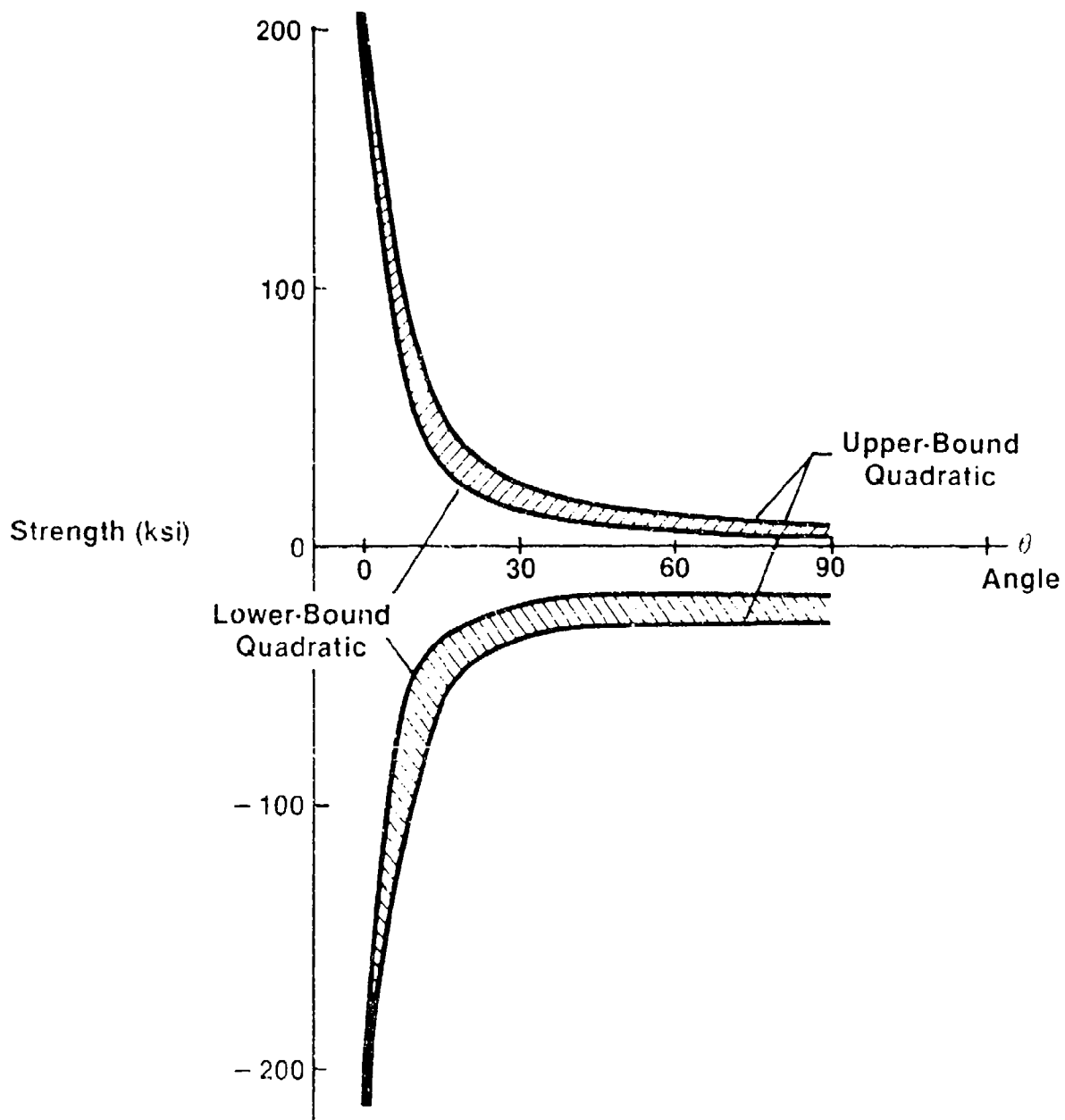
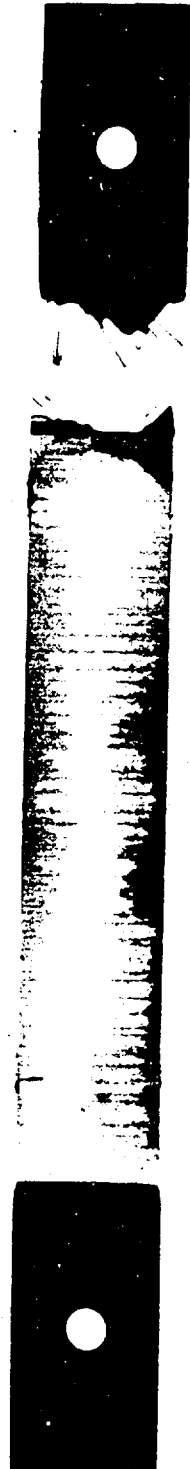


FIGURE 12 UNIAXIAL SPECIMENS THEORETICAL STRENGTH DIAGRAM



(a) SPECIMEN $(+45/90_2)_s$ STATIC TESTED AT $132^{\circ}\text{F}/50\% \text{ RH ENVIRONMENT}$



(b) SPECIMEN $(90_2/+45)_s$ STATIC TESTED AT $75^{\circ}\text{F}/50\% \text{ RH ENVIRONMENT}$



(c) SPECIMEN $(+45/90_2)_s$ STATIC TESTED AT $75^{\circ}\text{F}/50\% \text{ RH ENVIRONMENT}$

FIGURE 13. A RADIOGRAPHIC TECHNIQUE FOR GR/EP SPECIMENS

5.0 FATIGUE TESTS AND ANALYSIS

In the previous Phase II and Phase III programs, the mean fatigue strain data and strain amplitude for the $(+45/90_2)_S$ layup were developed as shown in Figures 14 through 17. In this Phase IV program, limited numbers of fatigue tests on $(+45/90_2)_S$ specimens were conducted to provide baseline data in comparing the original data (Phase II and Phase III data) to current data. The current fatigue tests of $(90_2/+45)_S$ were conducted at $75^\circ\text{F}/50\%$ RH environments and $132^\circ\text{F}/95\%$ RH to investigate the effect of layup sequence. The S-N data is shown in Figure 18 and strain histories are shown in Figures 19 through 22.

In order to have a fair assessment of the fatigue data, basic static test data from both the old batch of prepreg and current batch of prepreg is summarized in Table 11. Due to better static strength, the 55% fatigue stress level used for the Phase IV program is 12% higher than that in the Phase III program. The same is also true for the 50% stress level and 60% stress level. This difference in the basic data raises the question as to which are the reliable composite properties that can be used for micromechanics or other analysis. To understand the parameters that cause the variation of the composite property, a compilation of test data for AS-graphite/epoxy materials was made and the property list is shown in Table 12. The disparity among basic properties from different research sources for the same material prompts the necessity in looking into the micromechanics aspect. Relationships between fiber, matrix and composite as illustrated in Figures 3 and 4 can be utilized to estimate the properties of the fiber from the measured composite data. The results are shown in Table 13 together with the data obtained by Arenburg⁷ and Crane and Adams.⁸ In the calculations for Table 13, Poisson's ratio ν_{23} was obtained from E_2 and G_{23} in the isotropic plane. Based on the results in Table 13 and micromechanical relationships in Figures 3 and 4, variations of composite test data seem to come from three possible areas: 1) variation of fiber property from batch to batch; 2) variation of matrix characteristics from batch to batch; and 3) inconsistency in precise layup and cure processing which will result in changes, from panel to panel, of fiber

10⁵ 10⁶

10⁴ 10³

10²

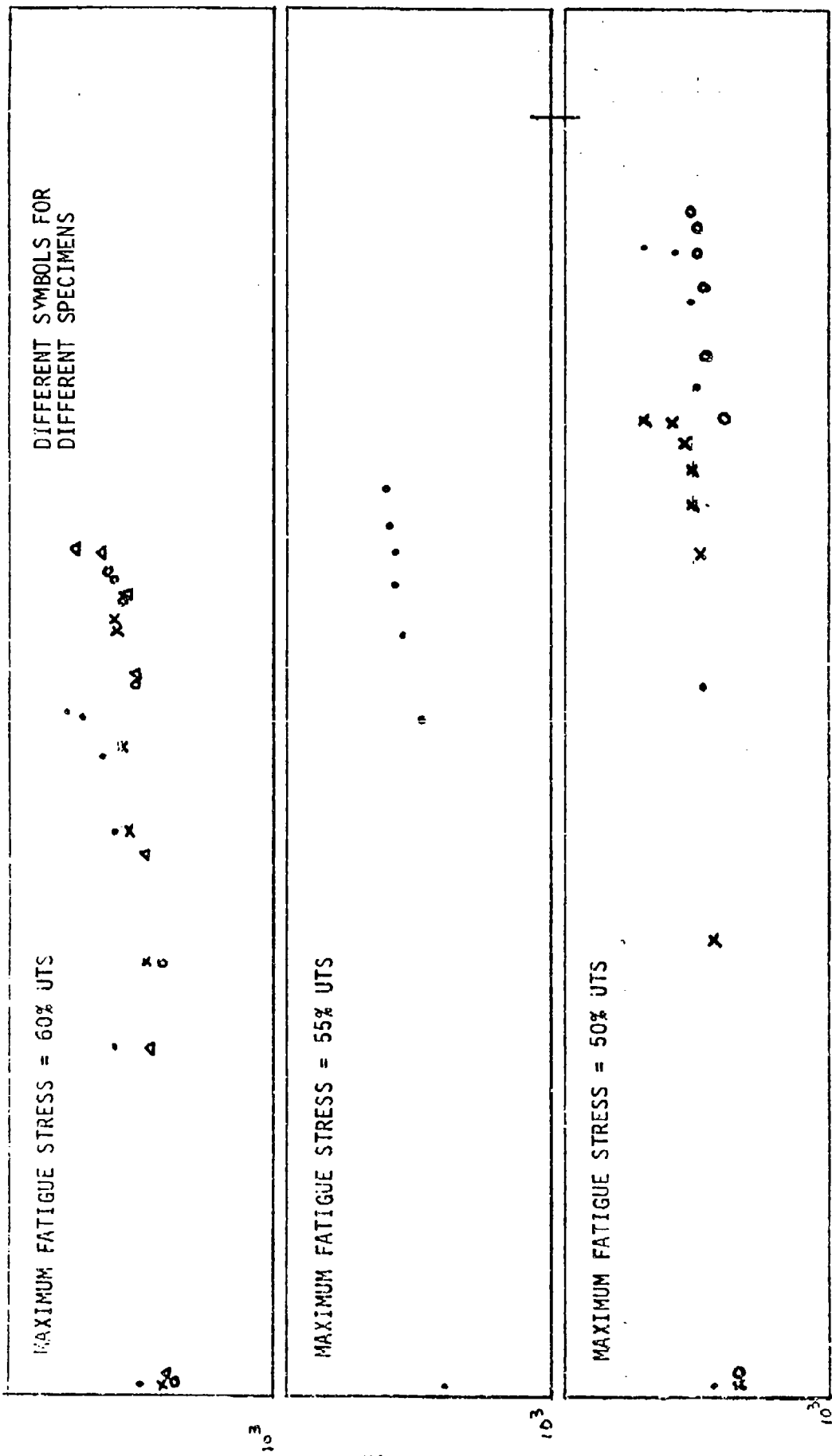


FIGURE 14. MEAN FATIGUE STRAIN CURVE OF (+45/90)₂ SPECIMEN AT 75°F/50% RH ENVIRONMENT

10⁶

10⁴

10³

10²

10¹

DIFFERENT SYMBOLS FOR DIFFERENT SPECIMENS

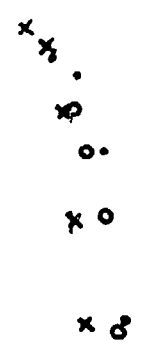
MAXIMUM FATIGUE STRESS = 60% UTS



MAXIMUM FATIGUE STRESS = 55% UTS



MAXIMUM FATIGUE STRESS = 50% UTS



NUMBER OF CYCLES, N

FIGURE 15. MEAN FATIGUE STRAIN CURVE OF (+45/90)₂ SPECIMEN AT 132°F/50% RH ENVIRONMENT

MEAN STRAIN, ϵ (10^{-4})

10² 10³ 10⁴ 10⁵ 10⁶

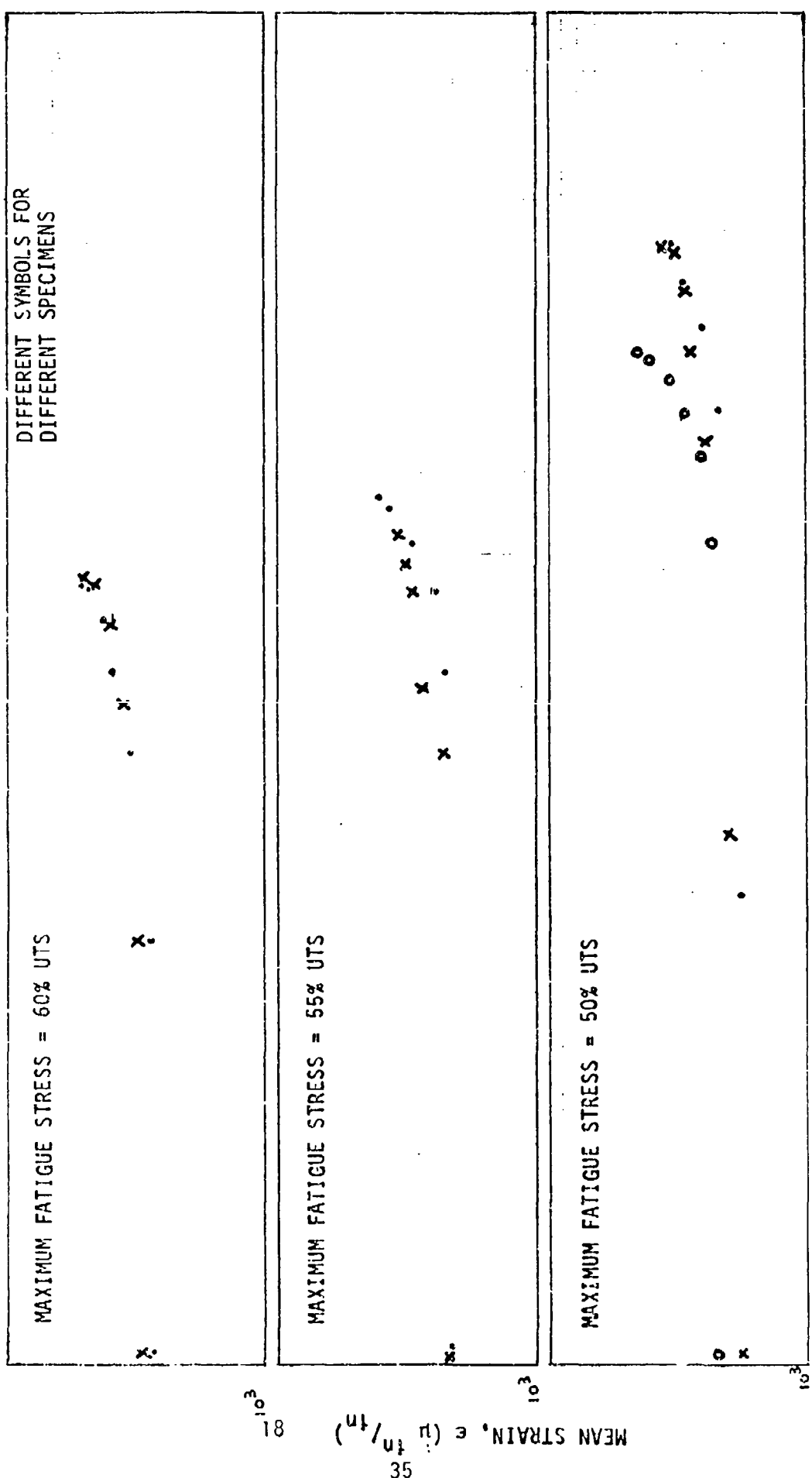
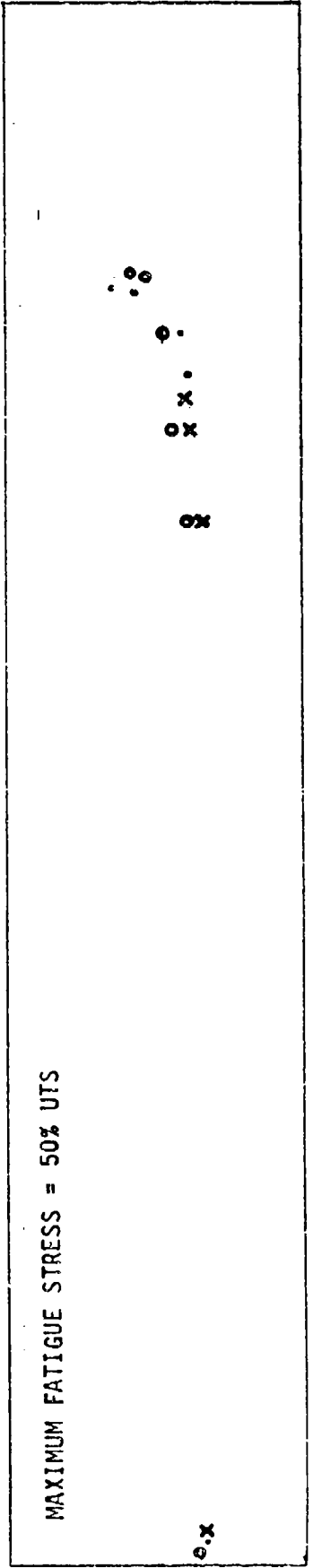
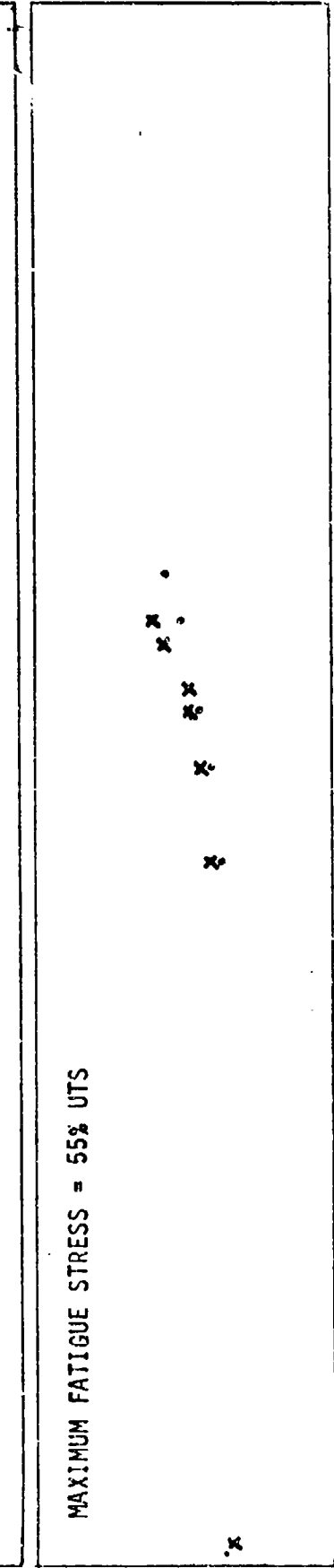
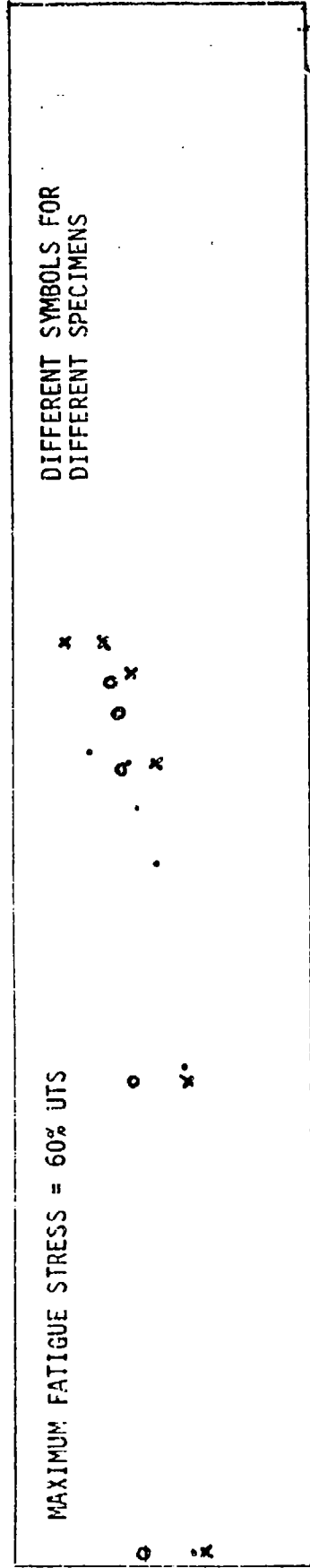


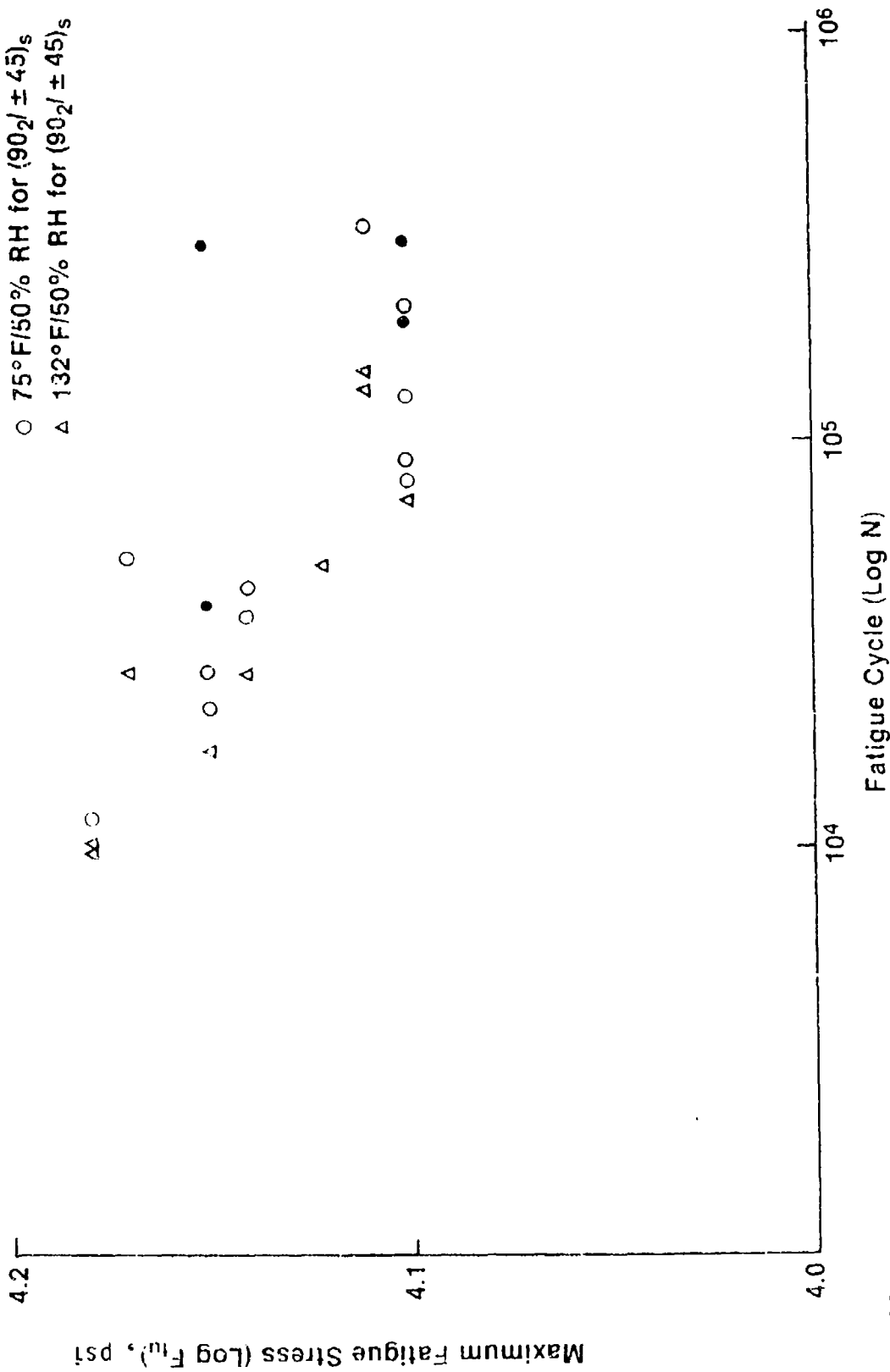
FIGURE 16. MEAN FATIGUE STRAIN CURVE OF (+45/90)_s SPECIMEN AT 132°F/95% RH ENVIRONMENT



NUMBER OF CYCLES, N

FIGURE 17. MEAN FATIGUE STRAIN CURVE OF (+45/90)₂ SPECIMEN AT 170°F/50% RH ENVIRONMENT

- 75°F/50% RH for ($\pm 45/90_2$)_s
- 75°F/50% RH for ($90_2/\pm 45$)_s
- △ 132°F/50% RH for ($90_2/\pm 45$)_s



P3-110.5

FIGURE 18 S-N DATA OF ($\pm 45/90_2$)_s AND ($90_2/\pm 45$)_s SPECIMEN

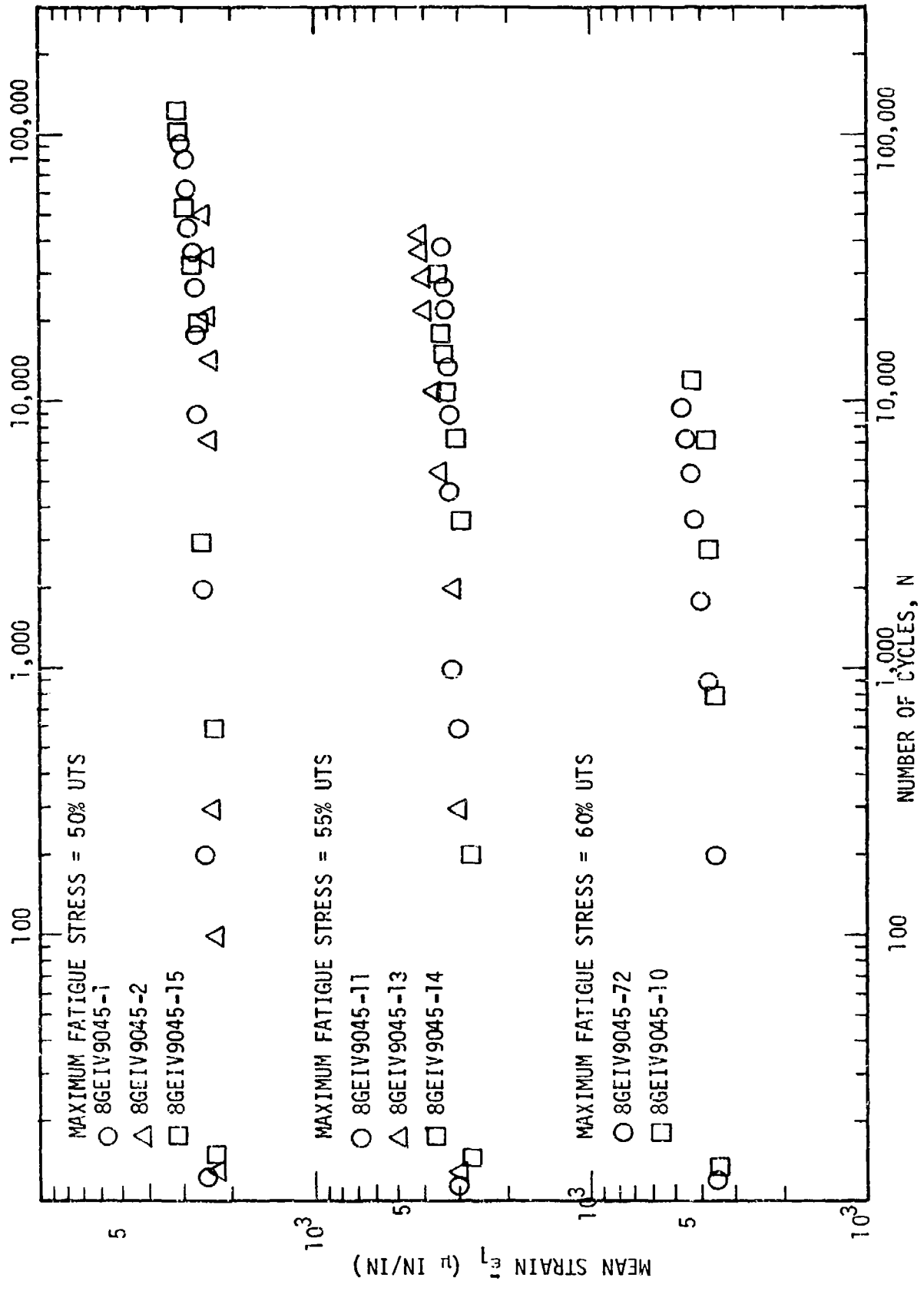


FIGURE 19 MEAN FATIGUE STRAIN CURVE OF (90₂/+45)_S SPECIMEN AT 75°F/50% RH

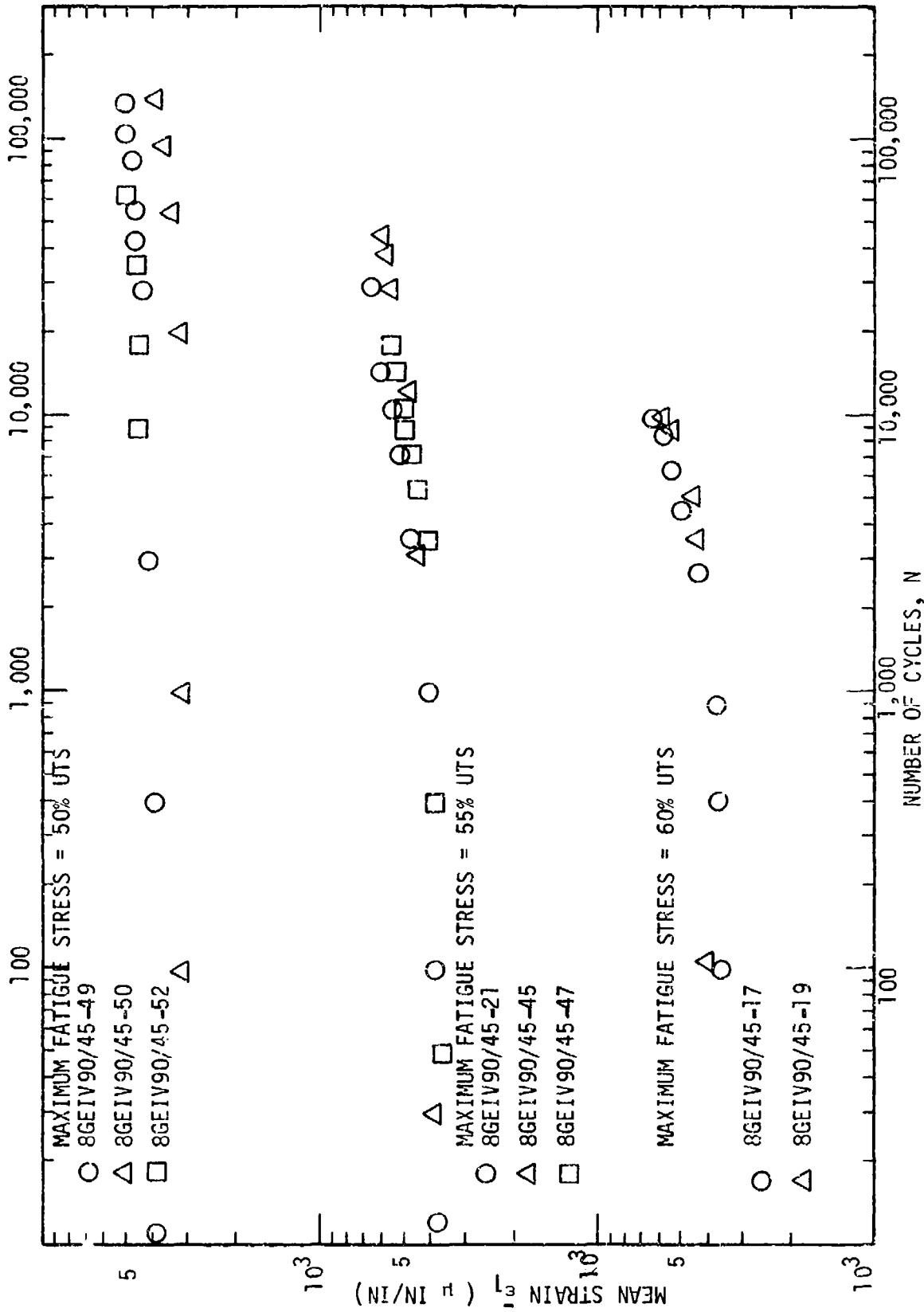


FIGURE 20 MEAN FATIGUE STRAIN CURVE OF (SC₂/+45)_s SPECIMEN AT 132°F/95% RH

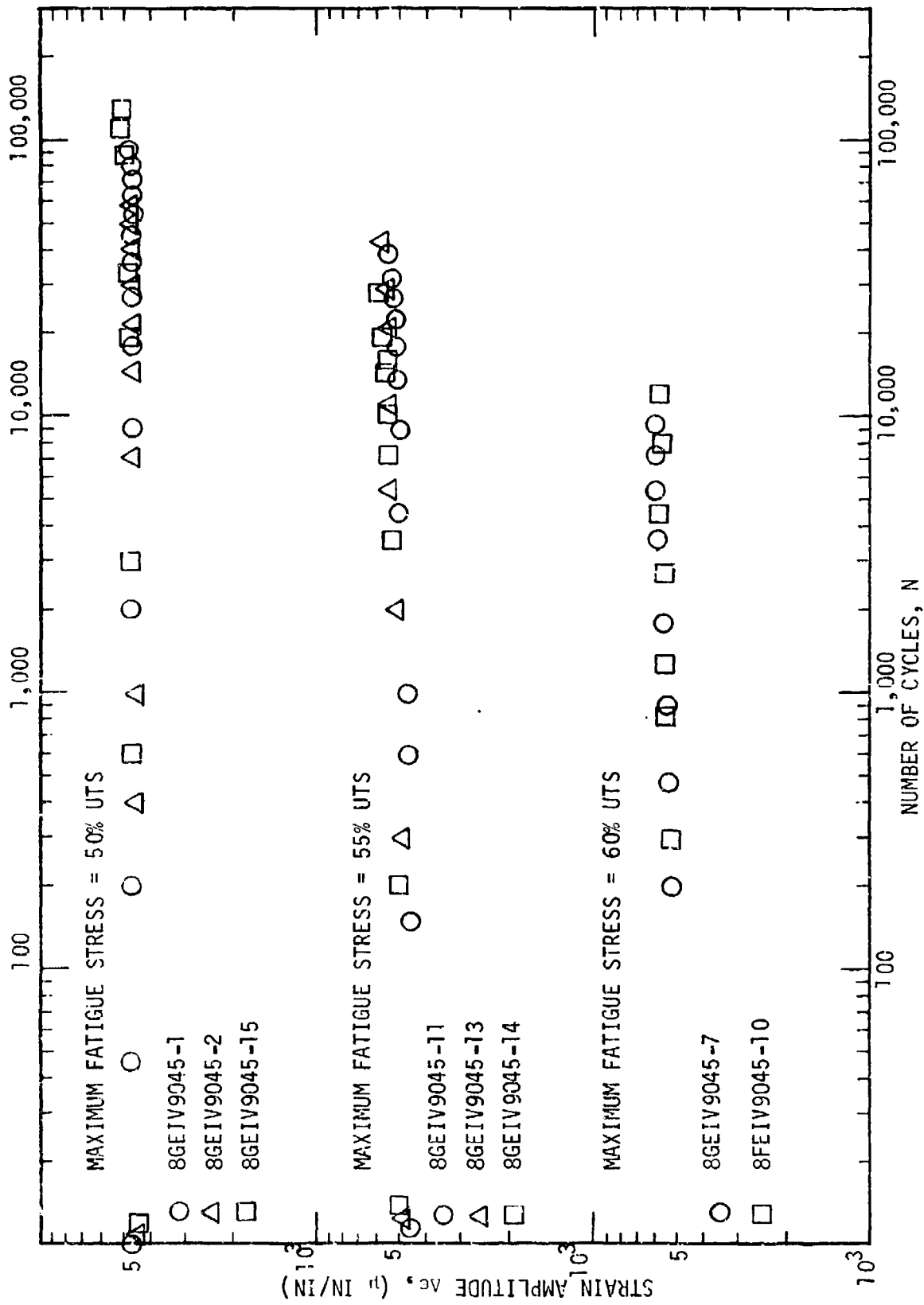


FIGURE 21 STRAIN AMPLITUDE OF $(90_2/+45)_S$ SPECIMEN AT 75°F/50% RH

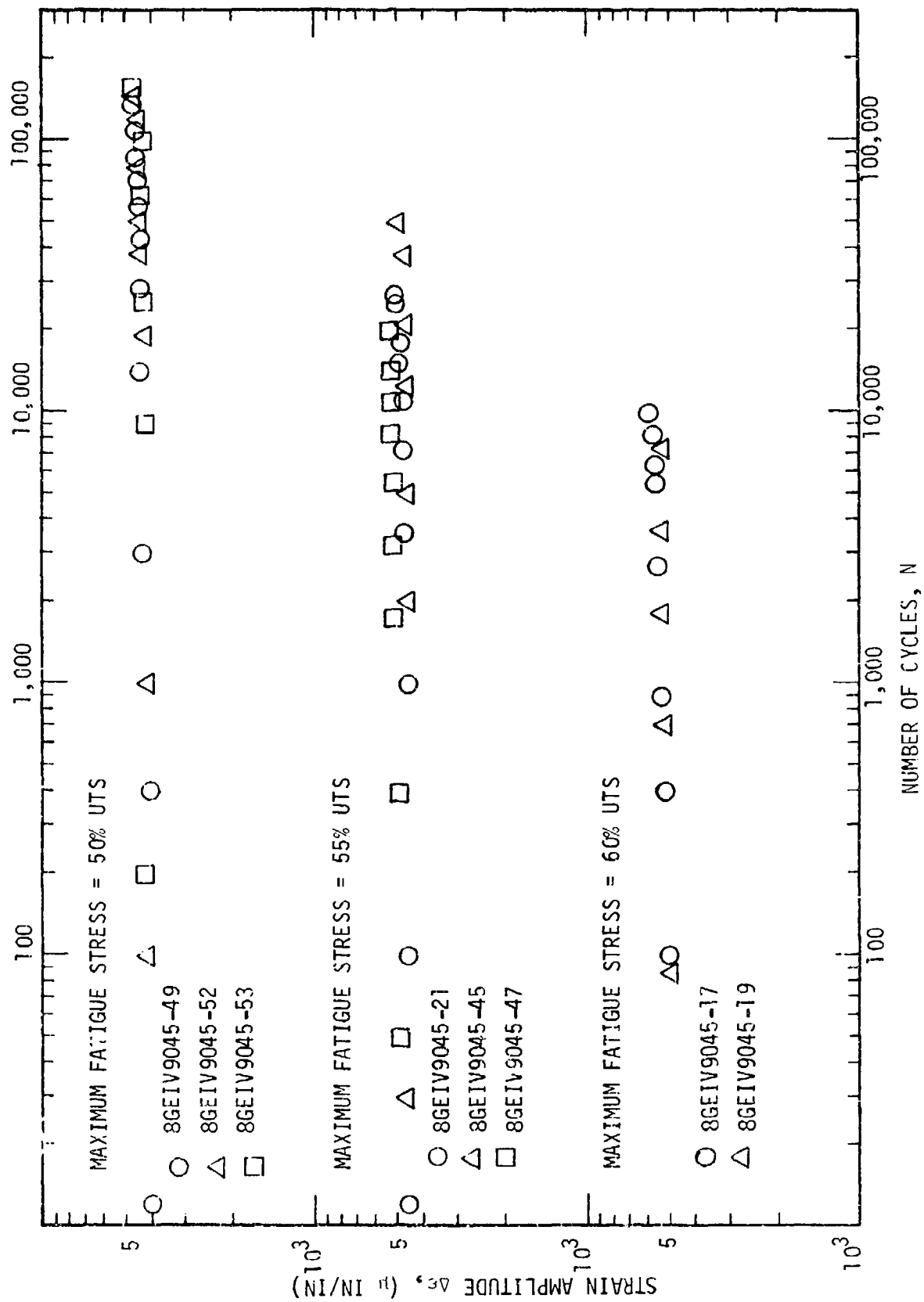


FIGURE 22 STRAIN AMPLITUDE OF $(90_2/+45)_S$ SPECIMEN AT $132^\circ\text{F}/95\% \text{RH}$

TABLE 11 MECHANICAL PROPERTIES OF (+45/90₂)_s LAMINATE
 IN PHASE III PROGRAM AND PHASE IV PROGRAM

ENVIRONMENT (°F/ % R.H.)	PERIOD WHEN DATA WERE GENERATED	ULTIMATE STRENGTH (F _{TU} , KSI)	ULTIMATE STRAIN (ε, μ in/in)	MODULUS (E, MSI)	FIBER VOLUME (%)
75/50	III	19.7	10500	2.78	68
	IV	23.1	12700	2.70	64
132/50	III	20.2	10450	2.79	68
	IV	24.6	13200	2.47	64
170/50	III	17.8	10900	2.66	68
	IV	23.2	12000	2.39	64

TABLE 12 TEST DATA OF AS-TYPE FIBER COMPOSITES

MECHANICAL PROPERTIES	RENTON AND HO (REFERENCE 1)	MONIB AND ADAMS (REFERENCE 3)	KNIGHT REFERENCE 6	TSAI-HAHN (REFERENCE 4)	(PHASE IV DATA)
COMPOSITE	AS/3501-6	AS/3501-6	AS/3502	AS/3501-6	AS/3501-6
E_1 , MSI	18.95	18.75	20.1	20.0	20.25
E_2 , MSI	1.47	1.55	1.60	1.30	1.40
G_{12} , MSI	0.85	0.964	0.878	1.03	0.752
G_{23} , MSI	-	0.51	0.548	-	-
ν_{12} , MSI	0.35	0.31	0.31	0.30	0.32
ν_{23} , MSI	-	0.49	0.52	-	-
ν_f (%)	62	-	-	66	64

TABLE 13 MICROMECHANICAL PROPERTIES OF AS-TYPE FIBER COMPOSITES

MECHANICAL PROPERTIES	CRANE AND ADAMS (REFERENCE 8)	ARENBURG (REFERENCE 7)	HO (REFERENCE 9)	HO (REFERENCE 9)	PHASE IV DATA	
FIBER	E_1 , MSI	31.9	29.87	30.16	28.6	30.85
	E_2 , MSI	2.02	2.61	2.86	4.2	3.21
	G_{12} , MSI	5.0	8.7	4.0	2.5	2.1
	G_{23} , MSI	0.8	0.98	0.854	0.89	1.02
	ν_{12}	0.2	0.265	0.2	0.32	0.30
	ν_{23}	0.25	0.33	0.674	0.36	0.59
	E_1 , MSI	0.619	0.667	0.66	0.66	0.66
	E_2 , MSI	0.619	0.667	0.66	0.66	0.66
MATRIX	G_{12} , MSI	0.229	0.239	0.244	0.244	0.244
	G_{23} , MSI	0.229	0.239	0.244	0.244	0.244
	ν_{12}	0.34	0.39	0.35	0.35	0.35
	ν_{23}	0.34	0.39	0.35	0.35	0.35
MATERIAL	AS/3501-6	AS/3501-6	AS/3501-6	AS/3501-6	AS/3501-6	
COMPOSITE	E_1 , MSI	20.17	18.98	19.83	18.82	20.25
	E_2 , MSI	1.244	1.51	1.35	1.54	1.40
	G_{12} , MSI	0.85	0.92	0.906	0.805	0.752
	G_{23} , MSI	0.46	0.51	0.502	0.51	0.54
	ν_{12}	0.25	0.31	0.25	0.33	0.32
	ν_{23}	0.36	0.47	0.345	0.51	0.30
V_f (%)	62	62	65	65	64	

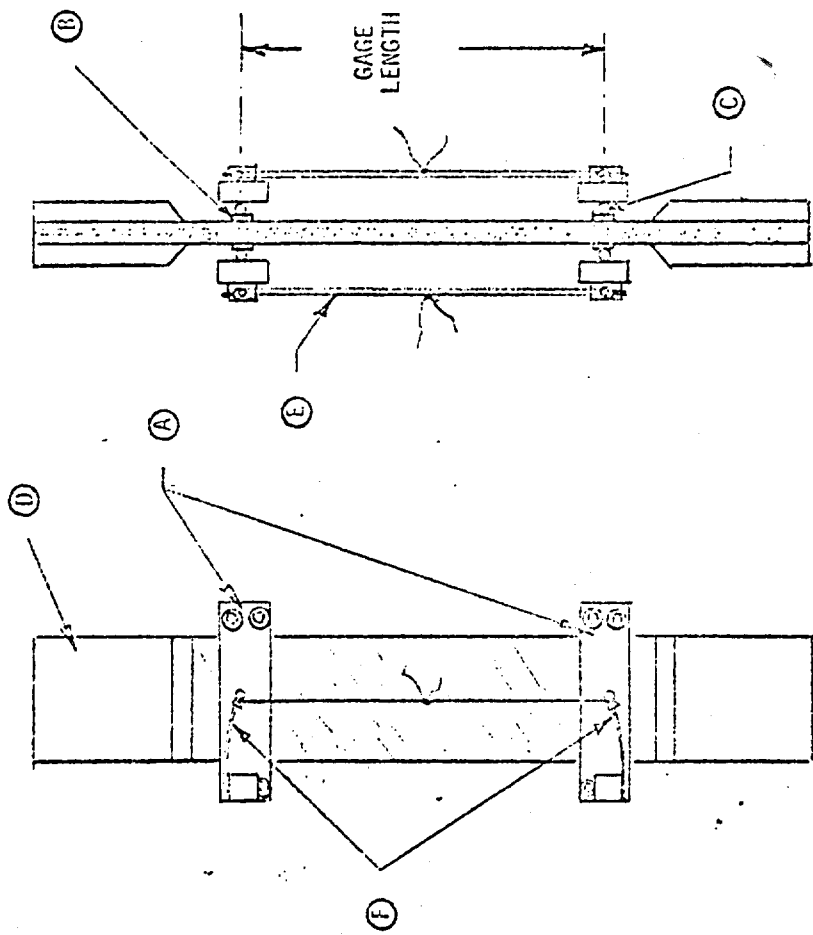
volume content, volatile content, and void content. Based on these observations, fatigue data and fatigue analysis needs to be associated with the individual batch properties. For present analysis purposes, the data in the last column of Table 13 were used.

6.0 RESIDUAL STRENGTH TESTS AND DELAMINATION TESTS

Residual strength tests and delamination tests on $(+45/90_2)_s$ specimens were conducted to study the interaction among matrix degradation, edge cracking/ply delamination and intraply cracking. This was done jointly with the Mechanics and Materials Center at Texas A&M University where they have a similar interest on the subject under an Air Force contract F49620-82-C-0057. The Phase IV program provided Texas A&M University ten residual strength specimens and thirty-six delamination specimens for testing. In return, Texas A&M University provided the Phase IV program results of their findings.

During testing at A&M University, strain measurement was made by using an extensometer called an "Elastic Strain Ratio Translator" (ESRT) gage. This ESRT extensometer was developed by B. C. Harbert of A&M University and its description is shown in Figure 23. Vought used the extensometer with two LVDTs as described in Figure 9.

The test procedure for the residual strength tests is shown in Figure 24. Although Vought and A&M used slightly different procedures, it involved essentially the same test steps: static preload, fixed duration of fatigue cycling and gradually increased static loading to failure. Tests were conducted at $75^{\circ}\text{F}/50\% \text{ R.H.}$ and $132^{\circ}\text{F}/50\% \text{ R.H.}$ environments and two fatigue stress levels, 55% of F_{tu} and 60% of F_{tu} . Test results obtained by Vought are summarized in Tables 14 and 15. Fatigue cycling was shown to have degradational effects on material stiffness and strength. It does not seem to affect the failure strain. Edge cracking was monitored during the residual strength test by using thin replicating tape. The typical positive prints from the replication technique are shown in Figure 25. Transverse cracks across the four 90° layers and delamination along the interface between the 90° layer and 45° layer are the two common crack formations along the edges. The replication technique was used to monitor the cracking formation and results are shown in Tables 16 and 17. At low fatigue stress levels (55% of F_{tu}), transverse cracking occurs earlier than delamination. At a higher stress level (60% of F_{tu}), the delamination cracks occur first.



(A) STAINLESS STEEL GAGE CLAMPS SECURED TO TEST SPECIMEN AT TWO LOCATIONS.
GAGE LENGTH DETERMINED BY ON CENTER DISTANCE BETWEEN CLAMPS

(B) KNURLED STEEL PRESSURE FOOT

(C) HARDENED STEEL BALL

(D) TYPICAL "TABBED" END UNIAXIAL TEST SPECIMEN

(E) ELECTRICAL RESISTANT STRAIN LOOP

(F) CANTILEVER LOADING SPRING

Reproduced From
Best Available Copy

FIGURE 23. ELASTIC STRAIN RATIO TRANSLATOR (ESRT)

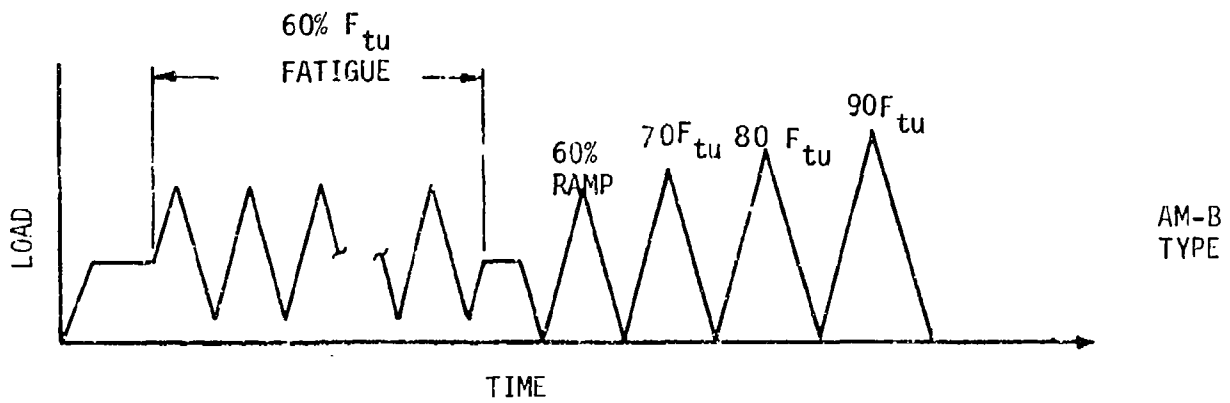
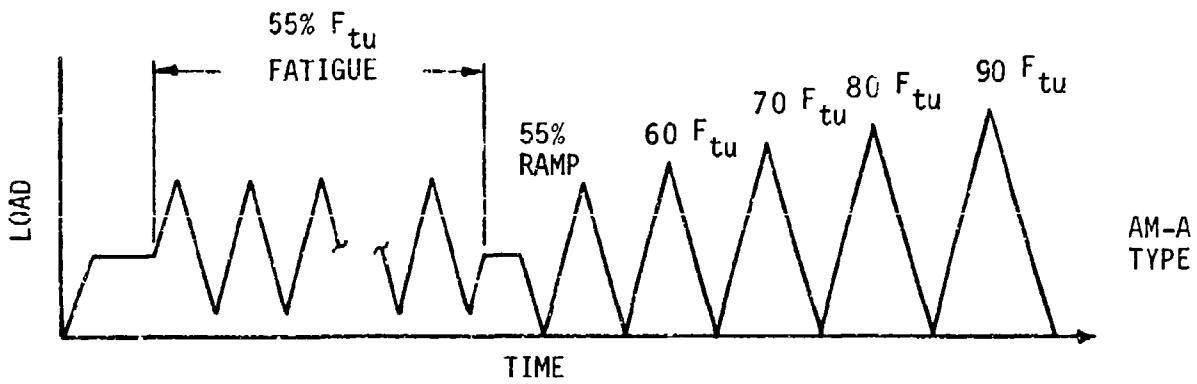
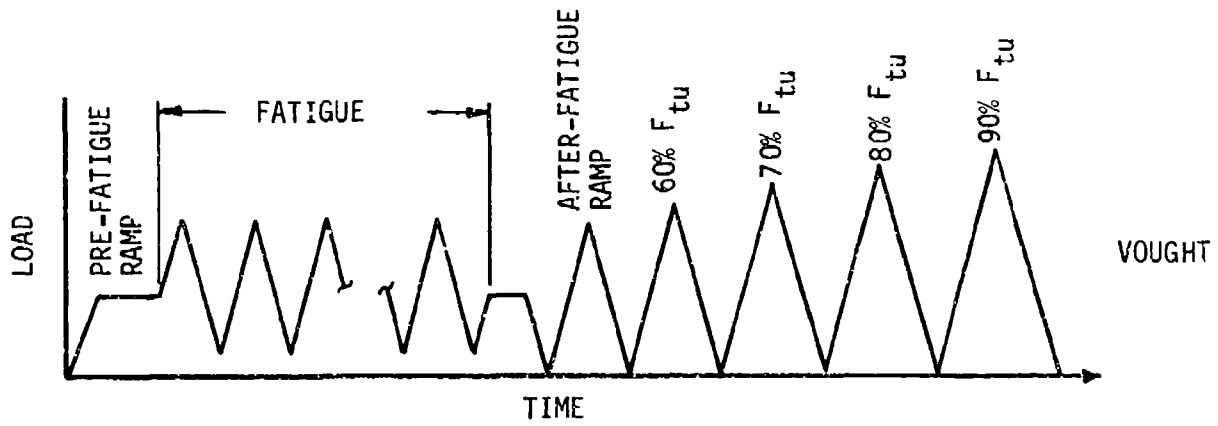


FIGURE 24 RESIDUAL STRENGTH TEST PROCEDURE

TABLE 14 RESIDUAL STRENGTH TEST SUMMARY IN 75°F/50% RH ENVIRONMENT

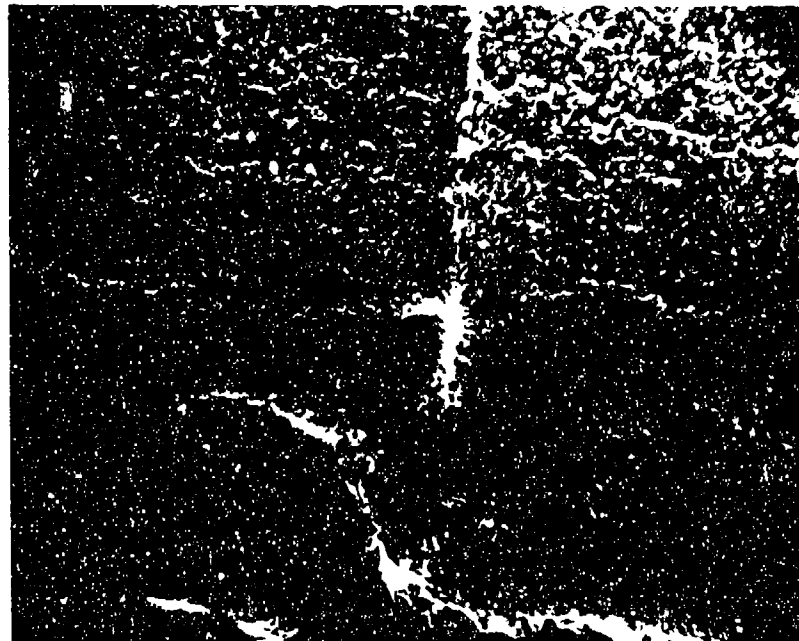
MAX. FATIGUE LOAD LEVEL (% OF F_{tu})	FATIGUE CYCLE	SPECIMEN ID	BEFORE FATIGUE	INITIAL MODULUS (MSI)	AFTER FATIGUE	FAILURE STRENGTH (KSI)	FAILURE STRAIN (M IN/IN)
55%	2,000	(+45/90) ₂ s -48	-	-	-	26.1	10400
		-56	-	-	-	25.5	11700
		-57	-	-	-	24.2	12200
	4,000	-49	-	-	-	26.1	11700
	7,000	-50	-	-	-	25.1	12400
		-1	3.12	2.53	24.5	12300	
60%	15,000	-51	-	-	-	25.1	12300
		-60	3.19	2.99	24.3	11700	
	1,000	-52	-	-	-	25.2	13300
	2,000	-53	-	-	-	25.1	12900
	4,000	-54	-	-	-	22.7	12900
		-6	2.99	2.46	21.2	12300	
	5,000	-3	3.03	2.50	22.9	12800	
	7,000	-55	-	-	-	21.4	12400
		-4	2.99	2.33	21.7	12700	

TABLE 15 RESIDUAL STRENGTH TEST SUMMARY IN 132°F/50% RH ENVIRONMENT

MAX. FATIGUE LOAD LEVEL (% OF F_{tu})	FATIGUE CYCLE	SPECIMEN ID	BEFORE FATIGUE	INITIAL MODULUS (MSI)	AFTER FATIGUE	FAILURE STRENGTH (KSI)	FAILURE STRAIN (IN/IN)
55%	1,000	(+45/90) ₂ s - 19	3.00	3.03	22.5	13900	
			3.11	2.78	21.6	13700	
			3.04	2.86	22.7	14400	
	4,000	- 20	2.98	2.66	21.9	12100	
			62	2.63	24.7	14800	
	7,000	- 21	2.72	2.56	21.9	12100	
24			2.33	19.8	13500		
25			2.56	22.2	15100		
60%	2,000	- 27	2.78	2.73	21.9	12900	
			28	2.44	21.8	11200	
			34	2.81	22.2	13200	
	3,000	- 29	2.70	2.70	21.5	13500	
			30	2.86	21.8	13300	
			31	2.92	21.4	14300	
			2.88	20.7	11500		



50X



200X

FIGURE 25. REPLICATION PRINTS OF EDGE CRACKING FOR SPECIMEN $(+45/90_2)_s$ AT 90% OF ULTIMATE LOAD

TABLE 16 DEVELOPMENT OF CRACKS FOR (+45/90₂)_s SPECIMENS AT 75°F/50% RH ENVIRONMENT

SPECIMEN ID	FAT. LOAD LEVEL	FAT. CYCLE	CRACKING							
			BEFORE FATIGUE	RIGHT AFTER FATIGUE	60% F _{tu}	70% F _{tu}	RAMP 80% F _{tu}	90% F _{tu}	100% F _{tu}	
-48	55%	2,000	-	-	T	T	T	T	T	T
-56	55%	2,000	-	-	-	-	-	-	-	-
-57	55%	2,000	-	-	-	-	-	-	-	-
-49	55%	4,000	-	-	-	-	T	T	T	T
-50	55%	7,000	-	-	D,T	D,T	D,T	D,T	D,T	D,T
-1	55%	7,000	-	-	T	T	T	T	D,T	D,T
-51	55%	15,000	-	-	T	T	T	T	T,D	T,D
-60	55%	15,000	-	-	T	T	T	T,D	T	T
-52	60%	1,000	D	T,D	T,D	T,D	T,D	T,D	T,D	T,D
-53	60%	2,000	-	-	T	T,D	T,D	T,D	T,D	T,D
-54	60%	4,000	-	T,D	T,D	T,D	T,D	T,D	T,D	T,D
-6	60%	4,000	-	D	T,D	T,D	T,D	T,D	T,D	T,D
-3	60%	5,000	-	D	T,D	T,D	T,D	T,D	T,D	T,D
-55	60%	7,000	-	D	T,D	T,D	T,D	T,D	T,D	T,D
-4	60%	7,000	-	T,D	T,D	T,D	T,D	T,D	T,D	T,D

D: DELAMINATION OBSERVED; T: TRANSVERSE CRACKS OBSERVED

TABLE 17 DEVELOPMENT OF CRACKS FOR (+45/90₂)_s SPECIMENS AT 132°F/50% RH ENVIRONMENT

SPECIMEN ID	FAT. LOAD LEVEL	FAT. CYCLE	CRACKING						
			BEFORE FATIGUE	RIGHT AFTER FATIGUE	RAMP				
					60% F _{TU}	70% F _{TU}	80% F _{TU}	90% F _{TU}	100% F _{TU}
-19	55%	1,000	-	-	T,D	T,D	T,D	T,D	
-22	55%	1,000	-	T,D	T,D	T,D	T,D	T,D	
-23	55%	1,000	-	-	T,D	T,D	T,D	T,D	
-20	55%	4,000	-	T,D	T,D	T,D	T,D	T,D	
-62	55%	4,000	-	-	T	T	T,D	T,D	T,D
-24	55%	4,000	-	T,D	T,D	T,D	T,D	T,D	
-25	55%	4,000	-	T,D	T,D	T,D	T,D	T,D	
-27	60%	2,000	-	T,D	T,D	T,D	T,D	T,D	T,D
-28	60%	2,000	-	T,D	T,D	T,D	T,D	T,D	
-34	60%	2,000	-	T,D	T,D	T,D	T,D	T,D	T,D
-35	60%	2,000	-	D	D	T,D	T,D	T,D	
-29	60%	3,000	-	T,D	T,D	T,D	T,D	T,D	
-30	60%	3,000	-	T,D	T,D	T,D	T,D	T,D	
-31	60%	3,000	-	T,D	T,D	T,D	T,D	T,D	
-33	60%	7,000	-	T,D	T,D	T,D	T,D	T,D	

D: DELAMINATION OBSERVED; T: TRANSVERSE CRACKS OBSERVED

Residual strength tests were also conducted by A&M University for regular $(+45/90_2)_s$ specimens and delamination specimens described in Section 3.0. Their test results are shown in Table 18. The typical data plots are shown in Figure 26 based on the test procedure AM-A type test of Figure 24. The hysteresis loops in the stress-strain curves are not obvious after the fatigue cycling and gradually open up under gradually increasing static loads. It was found from the results in Table 18 that center defects had a significant affect on the specimens' modulus and strength.

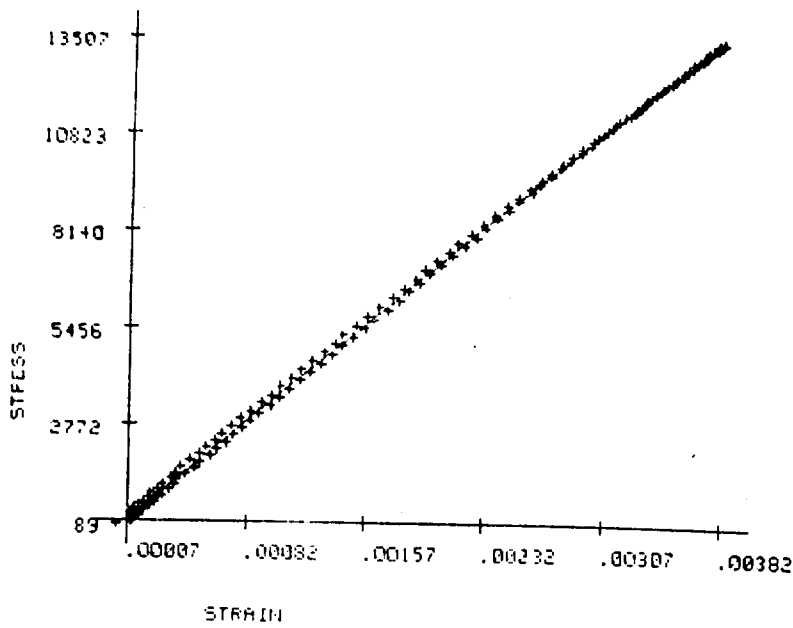
TABLE 18 RESIDUAL STRENGTH TESTS FOR (+45/90₂)_S DELAMINATION SPECIMENS

SPECIMEN ID	DEFECT LOCATION*	TEST ENVIRONMENT	TEST TYPE ⁺	FATIGUE CYCLE	MODULUS (MSI)					FAILURE LOAD (KSI)	
					PRE-FATIGUE RAMP	AFT-FATIGUE RAMP	60% F _{tu}	70% F _{tu}	80% F _{tu}		90% F _{tu}
4590-39	None		A	4000	3.16	3.17	3.21	3.11	3.13	2.83	24.8
4590-14	None		A	4000	-	3.20	3.12	3.02	3.20	-	24.6
4590-42	None		B	2000	3.30	3.06	3.06	3.07	3.04	2.95	24.3
11A	0.02" Brass Off ζ	75°F	A	4000	-	3.22	3.20	3.20	3.20	3.09	27.2
7A	0.02" Brass On ζ		A	4000	-	2.20	2.21	2.31	-	-	15.4
12A	0.02" Brass Off ζ		B	2000	2.98	2.99	2.99	2.91	2.90	2.95	24.2
3B	0.04" Brass Off ζ		A	4000	-	3.05	3.05	3.02	3.04	-	26.3
12B	0.04" Brass On ζ		A	4000	-	2.72	2.67	2.62	-	-	15.1
7B	0.04" Brass Off ζ		B	2000	3.25	3.25	3.25	3.27	3.23	3.21	24.5
4590-8	None		A	4000	3.37	3.37	3.37	3.37	3.25	2.91	24.5
4590-16	None		B	2000	3.04	2.97	2.97	3.00	2.90	2.77	23.5
6A	0.02" Brass Off ζ	132°F	A	4000	3.23	3.12	3.10	3.09	3.03	3.04	28.7
5A	0.02" Brass On ζ		A	4000	-	1.57	1.59	1.55	-	-	15.0
1A	0.02" Brass Off ζ		B	2000	2.95	2.91	2.91	2.92	2.95	2.88	27.1

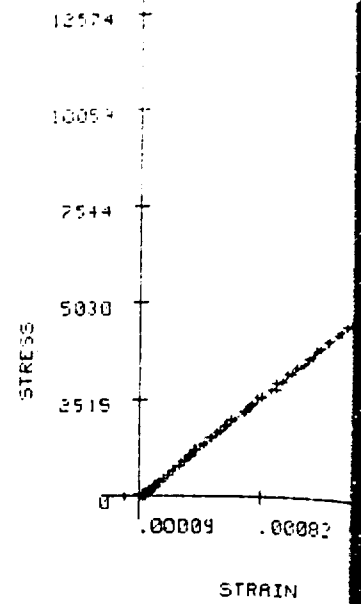
* REFER FIGURE 8 FOR DEFECT LOCATIONS

+ REFER FIGURE 24 FOR TEST TYPE

C RELATIVE HUMIDITY NOT CONTROLLED

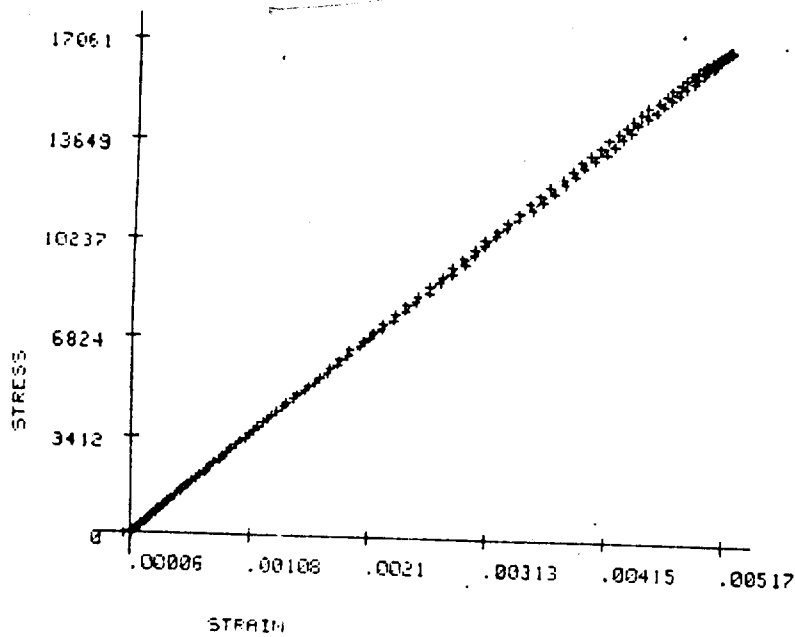


(a) RAMP TO 55% F_{tu} BEFORE FATIGUE CYCLING

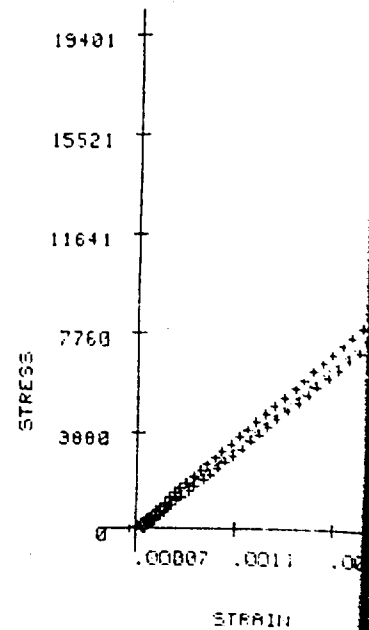


(b) RAMP TO 55%

Reproduced From
Best Available Copy

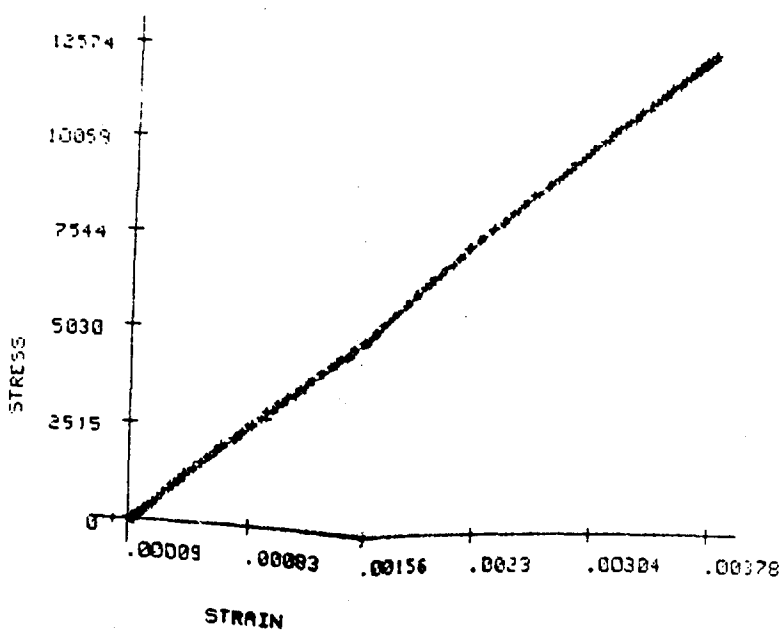


(d) RAMP TO 70% AFTER FATIGUE CYCLING

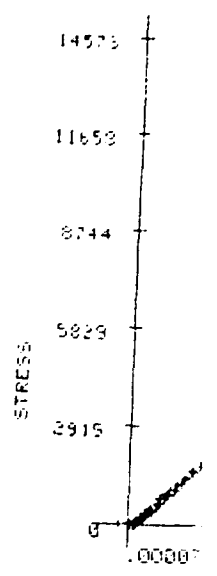


(e) RAMP TO 80%

FIGURE 26 TYPICAL STRESS-STRAIN CURVES

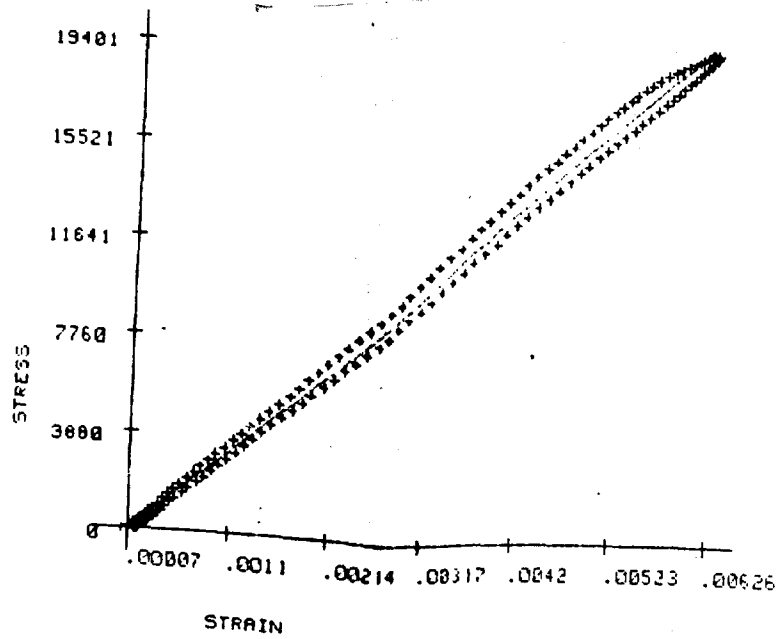


(b) RAMP TO 55% F_{tu} AFTER FATIGUE CYCLING

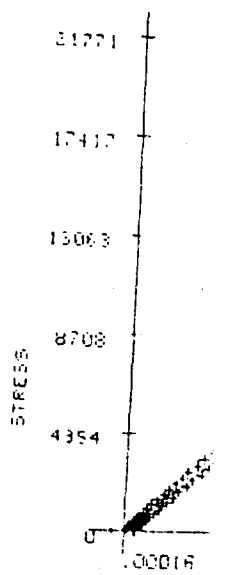


(c) RAMP TO 55% F_{tu} AFTER FATIGUE CYCLING

Reproduced From
Best Available Copy



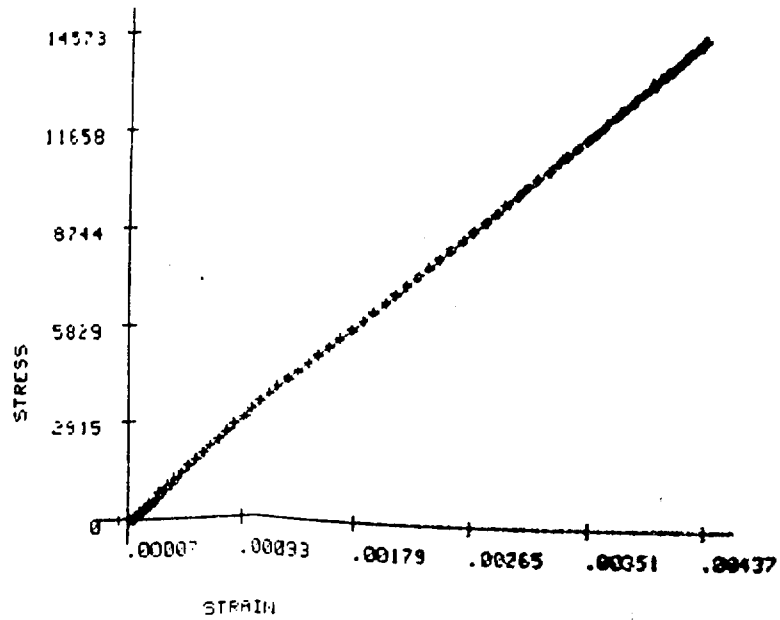
(e) RAMP TO 80% AFTER FATIGUE CYCLING



(f) RAMP TO 80% AFTER FATIGUE CYCLING

FIGURE 26 TYPICAL STRESS-STRAIN CURVES AT VARIOUS STAGES OF THE RESIDUAL STRENGTH TEST

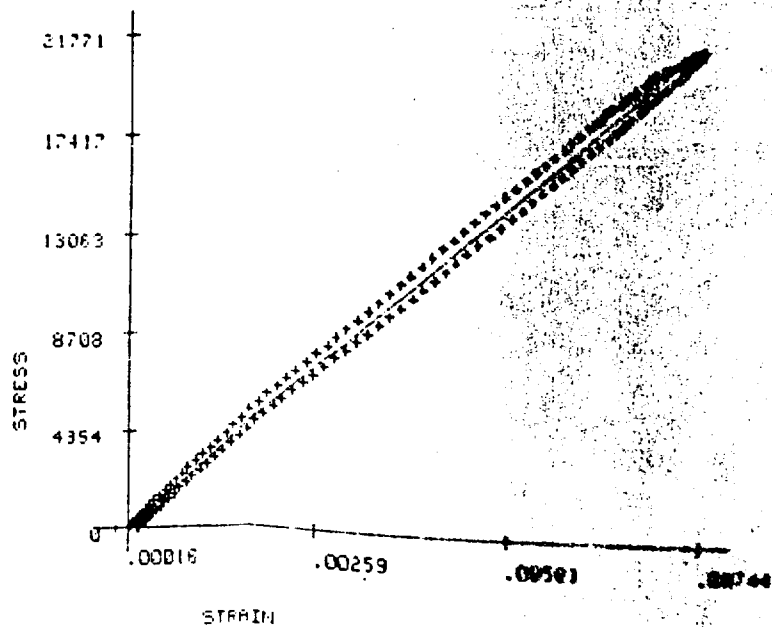
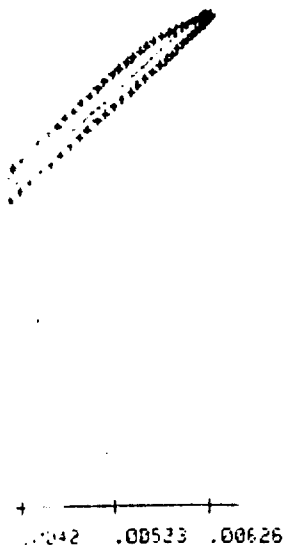
2



ER FATIGUE CYCLING

(c) RAMP TO 60% F_{tu} AFTER FATIGUE CYCLING

Reproduced From
Best Available Copy



TIGUE CYCLING

(f) RAMP TO 90% AFTER FATIGUE CYCLING

US STAGES OF THE RESIDUAL STRENGTH TEST

3

7.0 ANALYSIS OF DAMAGE GROWTH AND FAILURE

In the Phase III report, a theoretical model based on matrix degradation was proposed for estimating the uniaxial laminate failure strain in static and fatigue loading and for predicting fatigue life. Specifically, it was shown that by using a matrix modulus of approximately 10% of its initial (undamaged state) value, theoretically predicted strains were close to those at failure in static and fatigue tests. Although many of the failed coupons exhibited considerable delamination, it was suggested that any significant amount of delamination occurred primarily in the latter stages of failure and was triggered by gross matrix damage within plies.

These ideas have been further investigated as part of the Phase IV effort. In this section we consider in more detail the separate effects of matrix damage and delamination, and indicate possible ways in which they interact to produce overall failure. Since writing the Phase III report, some related studies have been published by others¹⁰⁻¹³ which are very informative on the nature of intraply damage and delamination in laminates similar to ours. This information, as well as some recent theoretical work,^{14,7} will be taken into account in this section.

7.1 DAMAGE THEORY FOR LINEAR ELASTIC COMPOSITES

According to the theory of linear elastic fracture mechanics, growth of a crack initiates when the so-called energy release rate G exceeds a critical value, G_c . This critical value is material-dependent and, in general, depends on environmental factors such as temperature and moisture content in the case of plastics. Thus, an important aspect of damage growth analysis is the prediction of energy release rates when cracks represent at least part of the damage. As there is considerable evidence that any significant damage in advanced polymeric composites usually consists of intraply and delamination cracks,¹⁰⁻¹³ we shall discuss the prediction of G for both types of cracking. Extension of the results to viscoelastic behavior is then made using existing theory.

Consider a tensile specimen in which the applied axial load is F and the associated axial displacement between the points of load application is U . Assuming linear elastic behavior for a fixed state of damage,

$$F = kU \quad (4)$$

where k is the stiffness. In general, k is a function of damage, which shall be represented by a set of N crack surface areas A_i ($i=1, \dots, N$). Neglecting residual strain energy, the total strain energy in the coupon is

$$W_T = 1/2 kU^2 \quad (5)$$

where $k = k(A_i)$. The familiar equation for energy release rate is obtained by forming the derivative of W_T with respect to A_i ,

$$G_i \equiv - \frac{\partial W_T}{\partial A_i} = - \frac{1}{2} \frac{\partial k}{\partial A_i} U^2 \quad (6)$$

where $k = k(A_i)$ and $i, j=1, 2, \dots, N$. Physically, $G_i dA_i$ (i not summed) is the work done by the elastic material on the failing material at the i th crack tip where the area of this crack increases by an infinitesimal amount dA_i . Inasmuch as U is constant when this change is evaluated, the externally applied forces do not work, and the entire change in strain energy dW_T is converted to mechanical work at the advancing crack tip. Strictly speaking, the notation which characterizes the shape and orientation of each existing crack and newly formed area should be used¹⁴. However, for present purposes it will be sufficient to use a simplified notation in which only the magnitudes of the areas A_i are explicitly identified.

Let G_{c_i} be the critical value of G_i , i.e., G_{c_i} is the "energy" (more precisely, the "mechanical work") per unit area required to separate material points at the crack tip associated with the new area dA_i . Whether or not the new surface dA_i is actually formed depends on whether or not the available energy G_i exceeds the required energy G_{c_i} ; i.e., if $G_i < G_{c_i}$ then $dA_i = 0$ and if $G_i > G_{c_i}$ then $dA_i > 0$.

By defining compliance, $C = i/k$, and using the relation $U = CF$, equation (6) may be rewritten in a similar form in terms of applied load,

$$G_i = \frac{1}{2} \frac{\partial C}{\partial A_i} F^2 \quad (7)$$

Equations (6) and (7) are standard forms for the energy release rate of specimens and structures when a single applied load and displacement are considered. In predicting G_i for specimens under original stress, it is often helpful to rewrite these equations in terms of effective axial modulus, E , overall or average stress and strain ϵ . Thus, with $\sigma = E\epsilon$, $\sigma = F/A_{CS}$ and $\epsilon = \frac{U}{L}$ (where A_{CS} = cross-sectional area and L = length of coupon prior to application of F), we obtain

$$k = EA_{CS}/L, \quad C = LD/A_{CS} \quad (8)$$

where $D = E^{-1}$ is the uniaxial compliance. Thus,

$$G_i = - \frac{V}{2} \frac{\partial E}{\partial A_i} \epsilon^2 \quad (9)$$

or, equivalently,

$$G_i = \frac{V}{2} \frac{\partial D}{\partial A_i} \sigma^2 \quad (10)$$

in which $V = A_{CS}L$ is the volume of the specimen.

In studies of the graphite/epoxy composite material T300/5208, which is very similar to the composite used here, O'Brien^{11,12} found that the modulus E of the laminates decreased linearly with the amount of delamination area A_d (as defined by the area projected onto the plane of the laminate through x-ray measurements). Thus, using O'Brien's notation for moduli,

$$E = (E^* - E_{LAM}) \frac{A_d}{A_{dT}} + E_{LAM} \quad (11)$$

where $A_{dT} = 2bL$ is the projected delaminated area of a fully delaminated sample of length L . Noting that $A_d = 0$ without delamination, and $A_d = A_{dT}$ with full delamination, equation (11) implies that

$$E_{LAM} = \text{specimen modulus without delamination}$$

$$E^* = \text{modulus of a fully delaminated specimen}$$

As an illustration of A_d and A_{dT} , consider the laminate in Figure 27, which shows the end view of a specimen with edge delaminations of depth A . If the depth were constant along the specimen length L (x -direction), then $A_d = 2AL$. O'Brien assumed a pair of edge delaminations existed above and below the center plane of symmetry in analytical predictions of modulus; therefore, four crack tips (rather than the two in Figure 27) were assumed to be involved in the delamination process. However, A_d and A_{dT} are the same for the cases of two and four cracks in view of their definition.

Recall that the energy release rate G_i is the mechanical work available at a crack tip per unit of new area at this one tip; thus, only one crack tip is advanced when calculating the derivative E/A_i in Equation (9). With this point in mind, let us first consider the two-crack case in Figure 27, in which we let $i = 1$ and $i = 2$ represent the two cracks, and E^*_2 the specimen modulus with full delamination. Using $A_d = A_1 + A_2$ and $A_{dT} = 2bL$ in Equation (11) for E , we then obtain from Equation (9) for $i = 1$,

$$G_1 = \frac{h^2}{2} (E_{LAM} - E^*_2) \quad (12)$$

In the case of four cracks where the cracks extending from the same edge have the same depth, one has $A_d = (A_1 + A_2 + A_3 + A_4)/2$ and $A_{dT} = 2bL$; thus

$$G_1 = \frac{h^2}{4} (E_{LAM} - E^*_4) \quad (13)$$

Here, E^*_4 is modulus when the specimen is fully delaminated.

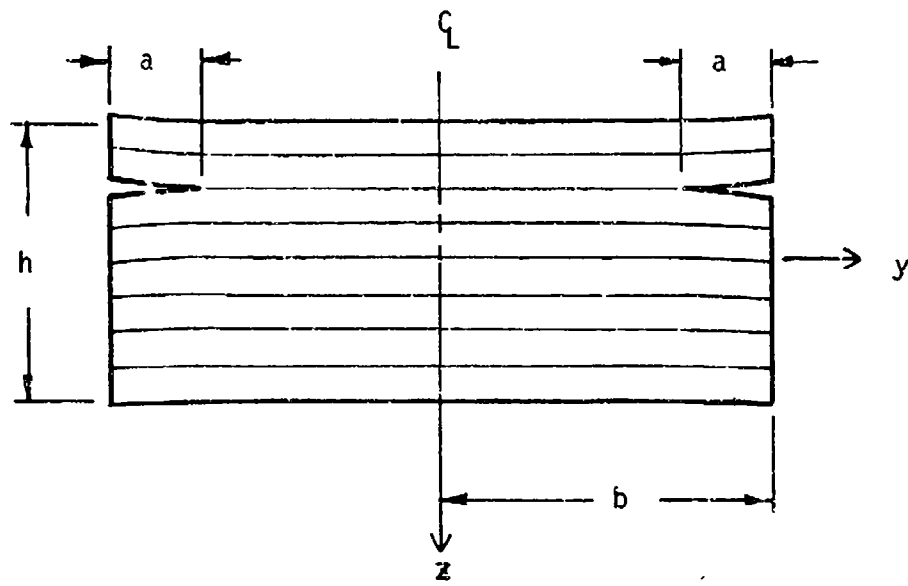


FIGURE 27. END VIEW OF TENSILE SPECIMEN WITH A PAIR OF DELAMINATION CRACKS OF EQUAL DEPTH a .

The value of energy release rate is the same for each of the two cracks (Equation (12)) or each of the four cracks Equations (13). Furthermore, these two equations are really not restricted to equal or uniform crack depths. Namely, each crack could have a different depth and it could vary along the length; indeed, lengthwise variation was observed.¹¹ Although the formula for G_i is independent of depth (because E is linear in delamination area), it does depend on the number of delamination cracks (through factor 1/2 or 1/4 and the value of E^*_2 or E^*_4). O'Brien's predictions were based on Equation (12), but with E^*_4 used in place of E^*_2 . This resulted in the best agreement for measured stiffness changes and the critical value of G_i . The need for this modification of the basic formula for G_i is probably due to the presence of many cracks within each ply, which were not accounted for in predicting E_{LAM} and E^* , and their participation in forming the delamination crack tips; these intralaminar cracks are shown and discussed in detail in References 10 and 11. O'Brien found that essentially only one delamination grew from each edge, but it skipped from one side of the center plane to the other through transverse cracks.

The effect of intralaminar cracks on both E_{LAM} and E^* will be considered here. First, however, we shall make some comparisons using Equations (12) and (13) which provide evidence for the fact that static and fatigue failure behavior reported on the program cannot be explained without accounting for them.

The modulus E_{LAM} without damage for the $[\pm 45/90_2]_S$ laminate has been predicted elsewhere in this report (Figure 11); the largest and smallest values, based on the extremes of constituent properties for all environments studied, are 3.38 and 3.17×10^6 psi. The modulus with full delamination E^* will be predicted using classical lamination theory for several cases; Jones' notation¹⁵ is employed. For a laminate in terms of the coordinates in Figure 27, the forces $N = (N_x, N_y, N_{xy})$, moments $M = (M_x, M_y, M_{xy})$,

middle surface strains $\epsilon^0 = (\epsilon_x^0, \epsilon_y^0, \gamma_{xy}^0)$ and curvatures $\kappa = (\kappa_x, \kappa_y, \kappa_{xy})$ are related according to

$$\begin{bmatrix} N \\ M \end{bmatrix} = \begin{bmatrix} A & B \\ B & D \end{bmatrix} \begin{bmatrix} \epsilon^0 \\ \kappa \end{bmatrix} \quad (14)$$

and, in the inverse representation,

$$\begin{bmatrix} \epsilon^0 \\ \kappa \end{bmatrix} = \begin{bmatrix} A' & B' \\ B' & D' \end{bmatrix} \begin{bmatrix} N \\ M \end{bmatrix} \quad (15)$$

The 6 x 6 symmetric matrices in Equations (14) and (15) are obviously inverses of one another, and are each comprised of three 3 x 3 symmetric matrices (A, B, D) and (A', B', D').

The modulus for uniaxial loading without delamination, E_{LAM} , is

$$E_{LAM} = (h A'_{11})^{-1} \quad (16)$$

where A'_{11} is the first element of the compliance matrix A'. The modulus with complete delamination, E^* , in which all of the n separated laminae (sublaminae) are under the same axial strain, is

$$E^* = \frac{1}{h} \sum_{i=1}^n E_i h_i \quad (17)$$

By definition,

$$E_i = N_{xi} / h_i \epsilon_x^0 \quad (18)$$

which is the axial modulus of the ith sublaminate, h_i is its thickness, and N_{xi} is the axial force on it.

It is not obvious what constraints or edge loadings should be used in predicting N_{xi} . O'Brien¹¹ assumed all three curvatures κ and edge forces N_{yi} and N_{xyi} are zero; this may be an acceptable application for some cases in view of the constraint imposed on out-of-plane deformations by the uncracked center section along the delamination crack tips and the alternating plane of delamination along the sample length observed. For zero curvatures and $N_{yi} = N_{xyi} = 0$,

$$E_i = (h_i A''_{11i})^{-1} \quad (19)$$

where A''_{11i} is the first element of the inverse of the submatrix A_i for the ith sublaminate. For relatively deep delaminations without any or many changes in the plane of delamination, significant curvatures of unbalanced and/or unsymmetric sublaminates may occur. As an extreme case, where each sublaminate is under no edge moments and forces other than N_{xi} , the axial modulus is

$$E_i = (h_i A'_{11i})^{-1} \quad (20)$$

where A'_{11i} is the first element of the matrix A' for the ith sublaminate.

The moduli (19) and (20) enable estimates of the energy release rate to be made. In order to obtain more accurate predictions, one should analyze the partially delaminated test specimen using plate theory or a more general approach, allowing for spatially varying strains and curvatures. However, this much more complicated problem will not be addressed here. Instead, we shall consider one more case, which is intermediate to the zero curvature

result, Equation (19), and unconstrained sublaminates, Equation (20). It is motivated by the problem in which delamination occurs along the center plane of the $[\pm 45/90_2]_s$ laminate. Assuming delaminations of equal depth extend from each edge, and that the depth is constant along the sample length, the zero curvature case, Equation (19) yields $E_i = E_{LAM}$; thus, the energy release rate is predicted as zero. In practice, an opening mode of crack displacement occurs, in which the curvature γ serves to define the amount of opening displacement. For a relatively long specimen, a reasonable assumption is that the out-of-plane displacements do not vary along the length, ($K_{xy} = K_x = 0$), and the free edge forces and moments are zero ($N_y = N_{xy} = M_y = M_{xy} = 0$). Inasmuch as E_x is specified to be the same for all sublaminates, one too many conditions have been specified; we shall drop the requirement $M_{xy} = 0$ in one problem, and drop $N_{xy} = 0$ in a second problem.

Moduli for the $[\pm 45/90_2]_s$ laminate: The center-plane delamination problem will be discussed first. For the constituent properties which result in the largest modulus, $E_{LAM} = 3.38 \times 10^6$ psi, we find

$$E^* = 2.42 \times 10^6 \text{ psi if } N_y = N_{xy} = M_y = K_x = K_{xy} = 0 \quad (21)$$

and only a slightly different value

$$E^* = 2.48 \times 10^6 \text{ psi if } N_y = M_{xy} = M_y = K_y = K_{xy} = 0 \quad (22).$$

Equation (21) provides a higher energy release rate than (22), and will be used in delamination predictions. For the fully unconstrained case, Equation (20),

$$E^* = 2.11 \times 10^6 \text{ psi} \quad (23)$$

Referring now to the problem illustrated in Figure 27, in which one pair of cracks exists between the -45 and 90 plys, we find for the properties corresponding to $E_{LAM} = 3.38 \times 10^6$ psi,

$$E^* = 2.80 \times 10^6 \text{ psi (based on Equation (19))} \quad (24)$$

and

$$E^* = 2.02 \times 10^6 \text{ psi (based on Equation (20))} \quad (25)$$

Next, in addition to the cracks shown in Figure 27, assume another pair of cracks exist between the 90 and -45 plys below the sample middle surface. Then

$$E^* = 2.03 \times 10^6 \text{ psi (based on Equation (19))} \quad (26)$$

and

$$E^* = 1.85 \times 10^6 \text{ psi (based on Equation (20))} \quad (27)$$

Critical axial strain for delamination of the $[\pm 45/90]_s$ laminate:

Equations (12) and (13) may be used to predict the strain at which delamination occurs, ϵ_c , given the critical value ϵ_c :

$$\epsilon_c = \left(\frac{2G_c}{h\Delta E} \right)^{0.5} \quad (2 \text{ cracks}) \quad (28)$$

$$\epsilon_c = \left(\frac{4G_c}{h\Delta E} \right)^{0.5} \quad (4 \text{ cracks}) \quad (29)$$

where, by definition

$$\Delta E = E_{LAM} - E^* \quad (30)$$

For the opening mode of delamination in the AS1/3501-6 composite in moderate environments, $G_c \simeq 1$ lb/in as reported by Wilkens.¹⁶ Mixed mode delamination G_c is higher, and a value of $G_c \simeq 2$ lb/in will be used here. (The measurements of G_c for mixed-mode cracking were made on unidirectional 0° fiber angle laminates, and it may be different for the laminate under study here.) Strains predicted from Equations (28) and (29) are listed below, in which the number in parenthesis corresponds to the particular E^* which was used in ΔE ; also, $E_{LAM} = 3.38 \times 10^6$ psi and $h = .044$ inches.

CASE	CRITICAL STRAINS (%)	E* EQUATION	G _c (lb/in)	NUMBER AND LOCATION OF CRACKS
1	.69	(21)	1	2, 90/90
2	.60	(23)	1	2, 90/90
3	.89	(24)	1	2, -45/90
4	1.26	(24)	2	2, -45/90
5	.58	(25)	1	2, -45/90
6	.82	(25)	2	2, -45/90
7	.82	(26)	1	4, -45/90
8	1.16	(26)	2	4, -45/90
9	.77	(27)	1	4, -45/90
10	1.10	(27)	2	4, -45/90

When the low values of constituent moduli are used, corresponding to $E_{LAM} = 3.17 \times 10^6$ psi, the critical strains are predicted to be less than those in the table, but only by a small amount; the ratio of these strains to those in the table is approximately 0.96.

It is instructive to compare the critical strains to those at which stiffness changes have been reported in the experimental studies for static and fatigue loading. In general, all of the predicted critical values are above those at which specimens begin to exhibit noticeable softening due to damage. Only for cases 2 and 5 do the strains approach the experimental values; but it is believed these predictions are unrealistically low as the sublaminates were assumed to be completely unconstrained. Also, except for samples with brass inserts at the middle plane, no significant delaminations at the middle surface were observed in failed coupons. In view of these observations, we estimate from the theory that $\epsilon_c \approx .7\%$ for the samples with centered brass, and $\epsilon_c \approx 0.8\%$ for the other samples; most delaminations appeared to occur between the -45 and 90° plies, regardless of whether or not brass separators were used between these plies. It should also be noted that the energy release rate during fatigue delamination of 0° laminates was close to the static critical

value G_c ,¹⁶ and therefore we have no basis at this time for using in Equations (28) and (29) an energy release rate which is significantly less than 1 lb/in.

Intraply Damage and Viscoelastic Effects: On the basis of the above estimates and the considerations in Phase III concerning the effect of a reduced matrix modulus, we believe intraply microcracking has to be taken into account besides delamination in order to predict the deformation and failure behavior of laminates; indeed, intraply damage may account for the largest amount of softening prior to failure in our specimens, considering how large the predicted critical strains without damage are. Measurements of damage using X-rays would be helpful to confirm the point. O'Brien¹¹ predicted that delamination caused more softening than intraply cracking in the laminates he studied, and this was supported by direct measurement of the amount of delamination.

The intralaminar cracking, as defined by parameters A_i , reduces E , Equation (11), in which both E_{LAM} and E^* are reduced by this cracking. Schapery¹⁴ developed a relatively general theory for elastic and viscoelastic materials (allowing for a distribution of G_i and A_i values) which could be used to account for the effect of strain history and viscoelastic properties on the damage and, in turn, its effect on moduli. However, explicit realistic predictions of damage are very involved, and will not be done here. This complexity exists whether or not viscoelastic effects are considered. For example, the stiffness E^* depends on not only the damage which occurs in the sublaminates after they are formed, but also on the damage prior to delamination and that produced by the high stresses around a delamination crack tip while it is moving and producing sublaminates. In the center part of a sample which is not delaminated, another complication exists because of the breakdown of classical lamination theory (CLT). Arenburg⁷ has shown that when the effective matrix modulus E_m is reduced from its initial value of 0.6×10^6 psi, interlaminar shear deformations may become important. For the $[\pm 45/90_2]_5$ specimens used in this program, energy release rates and stiffness predicted by CLT are in considerable error for damage states at the failure strains. This behavior seems to imply one should account for strain nonuniformity in the undelaminated part of the laminate in order to predict damage. Complex temperature dependence of G_c for mixed-mode cracking¹⁶ and residual stresses further complicate the problem.

8.0 CONCLUSIONS AND RECOMMENDATIONS

The effect of temperature and moisture on the deformation and failure behavior of AS/3501-6 uniaxial lamina and laminates is very complex. The commonly employed assumption of thermorheologically simple behavior for polymeric materials (in which changes in temperature and moisture simply alter the time-scale for response) is not valid. However, the Phase I studies indicated that creep and recovery strains of matrix-dominated specimens with a constant damage state can be characterized using a slightly generalized representation; namely, besides the environmental effect in the response time-scale, the environment affects the initial creep compliance. When the damage state changes continuously, as in the fatigue tests, it has not been possible to account for temperature and moisture effects in any simple way. The S-N curves for a given lamina or laminate can be approximated by a straight line using log-log axes, and in some cases (e.g., the $[\underline{+45/90}_2]_S$ laminate) the slope is the same for all environments studied. However, in general, the slope (i.e., the power law exponent) is different for different laminates. Also, in some cases an increase in temperature and/or moisture reduces the fatigue life, where in other cases it increases the fatigue life. It is believed this complex failure behavior is due at least in part to the delamination fracture toughness for the opening-mode increasing with increasing temperature, and for a mixed mode (with a large shearing component) exhibiting the opposite behavior.¹⁶

Intralaminar cracks appear to have a significant effect on the initiation and growth of delamination cracks. Theoretical estimates of energy release rates available to drive delaminations give values which are considerably below those required for their propagation unless interlaminar cracks are taken into account. It is thus believed that both types of damage have to be considered to predict deformation behavior of laminates with damage and to predict fatigue lifetimes. An approach using results from viscoelastic fracture mechanics theory is discussed. But, in order to develop and verify a realistic theoretical model, it appears necessary to make extensive use of NDI methods at various stages of specimen damage in order to identify the actual damage modes. A study of new specimen geometrics and fiber layups, taking into account data already generated, should be made in order to separate as much as possible distinct effects of intralaminar cracking, delamination, and residual stresses.

REFERENCES

1. Renton, W. J. and Ho, T., "The Effect of Environment on the Mechanical Behavior of AS/3501-6 Graphite/Epoxy Material," Final Phase I Report, NASC Contract No. N00019-77-C-0369, June 1978.
2. Ho, T., "The Effect of Environment on the Mechanical Behavior of AS/3501-6 Graphite/Epoxy Material, Phase II," ATC Report No. R-92100/9CR-61, Contract No. N00019-78-C-0599, January 10, 1980.
3. Ho, T. and Schapery, R. A., "The Effect of Environment on the Mechanical Behavior of AS/3501-6 Graphite/Epoxy Material, Phase III," NASC Contract No. N00019-79-C-0581, ATC Report No. R-92100/1CR-5, January 1981.
4. Tsai, S. W. and Hahn, H. T., "Introduction to Composite Materials," Technomic Publication, 1980.
5. Hashin, Z., "Analysis of Properties of Fiber Composites with Anisotropic Constituents," JOURNAL OF APPLIED MECHANICS, Vol. 46, Sept. 1979.
6. Knight, M., "The Determination of Interlaminar Moduli of Graphite/Epoxy Composites," 5th Mechanics of Composite Review, Dayton, Ohio, 1981.
7. Arenburg, R. T., "Analysis of the Effect of Matrix Degradation on Fatigue Behavior of a Graphite/Epoxy Laminate," Master Thesis, 1982, Civil Engineering, Texas A&M University.
8. Crane, D. A. and Adams, D. F., "Finite Element Micromechanical Analysis of a Unidirectional Composite Including Longitudinal Shear Loading," AMMRC TR 81-7, Army Materials and Mechanics Research Center, February 1981.
9. Ho, T., "The Effect of Environment on the Mechanical Behavior of AS/3501-6 Graphite/Epoxy Material, Phase IV," ATC Report No. R-92000/2CRL-10, March, 1982.
10. Reifsnider, K. L. and Jamison, R., "Fracture of Fatigue-Loaded Composite Laminates," Int. J. Fatigue, Oct. 1982, pp. 187-197.
11. O'Brien, T. K., "Characterization of Delamination Onset and Growth in a Composite Laminate," Damage in Composite Materials, STM STP 775, K. L. Reifsnider, Ed., American Society for Testing and Materials, 1982, pp. 140-167.
12. O'Brien, T. K., "The Effect of Delamination on the Tensile Strength of Unnotched, Quasi-Isotropic, Graphite/Epoxy Laminates," Proc. 1982 Joint Conf. on Experimental Mechanics, Hawaii, Society for Experimental Stress Analysis, May 1982, pp. 236-243.

13. O'Brien, T. K., Johnston, N. J., Morris, D. H., and Simonds, R. A., "A Simple Test for the Interlaminar Fracture Toughness of Composites," SAMPE Journal July/August, 1982, pp. 8-15.
14. Schapery, R. A., "On Viscoelastic Deformation and Failure Behavior of Composite Materials with Distributed Flaws," 1981 Advances in Aerospace Structures and Materials-AD-01, S. S. Wang and W. J. Renton, Eds., The American Society of Mechanical Engineers, Nov. 1981, pp. 5-20.
15. Jones, R. M., Mechanics of Composite Materials, Scripta Book Co., 1975.
16. Wilkins, D. J., "A Comparison of the Delamination and Environmental Resistance of a Graphite/Epoxy and a Graphite/Bismaleimide," Naval Air Systems Command Report NAV-GD-0037, Final Report, Sept. 1981.

DISTRIBUTION LIST

Commander
Naval Air Systems Command
Attn: AIR-5304
AIR-311
Washington, D.C. 20361

Commander
Naval Air Development Center
Attn: Code 606
Warminster, PA 18974

Commanding Officer
Naval Air Rework Facility
Attn: Code 340
Naval Air Station
Alameda, CA 94501

Commanding Officer
Naval Air Rework Facility
Attn: Code 340
Marine Corps Air Station
Cherry Point, NC 28533

Commanding Officer
Naval Air Rework Facility
Attn: Code 340
Naval Air Station
Jacksonville, FL 32212

Commanding Officer
Naval Air Rework Facility
Attn: Code 340
Naval Air Station
Norfolk, VA 23511

Commanding Officer
Naval Air Rework Facility
Attn: Code 340
Naval Air Station, North Island
San Diego, CA 92135

Commanding Officer
Naval Air Rework Facility
Attn: Code 340
Naval Air Station, Bldg 604
Pensacola, FL 32508

Director
Naval Research Laboratory
Attn: Codes 6383, 6654, 6120
Washington, DC 20375

Commander
Naval Sea Systems Command
Attn: Codes 051, 05D23
Washington, DC 20360

Director
Naval Ship R&D Center
Attn: Mr. M. Krenzke & Mr. A. Macander
Washington, DC 20034

Director
Naval Surface Weapons Center
Attn: Dr. J. Augl (R-31)
White Oak
Silver Spring, MD 20910

Office of Naval Research
Attn: Codes 431, 413
Washington, DC 20350

Air Force Wright Aeronautical Laboratories
Materials Laboratory
Attn: Codes LC, LN, LTF, LAE
Wright-Patterson AFB, OH 45433

Air Force Wright Aeronautical Laboratories
Materials Laboratory
Attn: Dr. J. M. Whitney/MBM
Wright-Patterson AFB, OH 45433

Army Materials & Mechanics Research Ctr
Dept of the Army
Attn: Library
Watertown, MA 02172

NASA Headquarters
Attn: Mr. C. F. Bersch
600 Independence Ave., S.W.
Washington, DC 20406

Distribution List (Cont'd)

NASA
Langley Research Center
Attn: Library
Hampton, VA 23665

NASA
Lewis Research Center
Attn: Library
Cleveland, OH 44185

Defense Technical Information Center
Cameron Station, Bldg #5
Alexandria, VA 22314

Director
Plastics Technical Evaluation Center
Picatinny Arsenal
Dover, NJ 07801

U.S. Applied Technology Laboratory
AVRADCOM
Attn: DAVDL-ATL-ATS
Fort Eustis, VA 23604

Brunswick Corporation
Technical Products Division
325 Brunswick Lane
Marion, VA 24354

Celanese Research Company
Box 1000
Attn: Mr. R. J. Leal
Summit, NJ 07901

E. I. DuPont de Nemours & Co.
Textile Fibers Dept
Wilmington, DE 19898

Fiber Materials, Inc.
Attn: Mr. J. Herrick
Biddeford Industrial Park
Biddeford, ME 04005

General Dynamics
Convair Aerospace Division
Attn: Tech Library
P. O. Box 748
Fort Worth, TX 76101

General Dynamics
Convair Division
Attn: Mr. W. Scheck
Dept 572-10
P. O. Box 1128
San Diego, CA 92138

General Electric
R&D Center
Attn: Mr. W. Hillig
Box 8
Schnectady, NY 12301

General Electric Company
Valley Forge Space Center
Philadelphia, PA 19101

B. F. Goodrich Aerospace & Defense Products
500 South Main St
Akron, OH 44318

Graftex Division
EXXON Industries
2917 Highwoods Blvd
Raleigh, NC 27604

Great Lakes Research Corporation
P. O. Box 1031
Elizabethton, TN 37643

Grumman Aerospace Corp
Attn: Mr. L. Poveromo
Bethpage, LI, NY 11714

Hercules Incorporated
Attn: Mr. E. G. Crossland
Magna, UT 84044

HITCO
1600 W. 135th St
Gardena, VA 90406

Illinois Institute of Technology
Research Center
10 West 35th St.
Chicago, IL 60616

Lear Fan Corp
P. O. Box 60,000
Reno, NV 89506

Distribution List (Cont'd)

Lockheed California Co.
Attn: Mr. J. H. Wooley
Box 551
Burbank, CA 91520

Lockheed-Georgia Co.
Attn: M. L. E. Meade
Marietta, GA 30063

Lockheed Missiles & Space Co.
Attn: Mr. H. H. Armstrong
Dept. 62-60
Sunnyvale, CA 94088

Material Sciences Corporation
1777 Walton Road
Blue Bell, PA 19422

McDonnell Douglas Corp.
McDonnell Aircraft Co.
Attn: Mr. J. Juergens
P. O. Box 516
St. Louis, MO 63166

McDonnell-Douglas Corp.
Douglas Aircraft Co.
Attn: Mr. R. J. Palmer
3855 Lakewood Blvd
Long Beach, CA 90801

North American Aviation
Columbus Division
4300 E. Fifth Ave
Columbus, OH 43216

Northrop Corp.
3901 W. Broadway
Attn: Mr. G. Grimes
Mail Code 3852-82
Hawthorne, CA 90250

Philco-Ford Corp
Aeronutronic Division
Ford Road
Newport Beach, CA 92663

Rockwell International Corp.
Attn: Mr. C. R. Rousseau
12214 Lakewood Blvd
Downey, CA 90241

TBW, Inc.
Systems Group
One Space Park
Bldg. 01, Rm 2171
Redondo Beach, CA 90278

TRW, Inc.
23555 Euclid Ave
Cleveland, OH 44117

Union Carbide Corporation
Chemicals & Plastics
One River Road
Bound Brook, NJ 08805

Union Carbide Corporation
Carbon Products Division
P. O. Box 6116
Cleveland, OH 44101

United Aircraft Corporation
United Aircraft Research Laboratories
E. Hartford, CT 06108

United Aircraft Corporation
Hamilton-Standard Division
Attn: Mr. T. Zajac
Windsor Locks, CT 06096

United Aircraft Corporation
Sikorsky Aircraft Division
Attn: Mr. J. Ray
Stratford, CT 06602

University of California
Lawrence Livermore Laboratory
Attn: Mr. T. T. Chiao
P. O. Box 808
Livermore, CA 94550

University of Maryland
Attn: Dr. W. J. Bailey
College Park, MD 20742

University of Wyoming
Mechanical Engineering Dept
Attn: Dr. D. F. Adams
Laramie, WY 82071

Westinghouse R&D Center
Attn: Mr. Z. Sanjana
1310 Beulah Road
Churchill Boro
Pittsburgh, PA 15235